STAT3-mediated allelic imbalance of novel genetic variant rs1047643 and B cell specific super-enhancer in association with systemic lupus erythematosus

Yanfeng Zhang[1*], Kenneth Day[2], Devin M. Absher[1*]

1. HudsonAlpha Institute for Biotechnology, Huntsville, AL 35806 USA

2. Zymo Research Corp, Irvine, CA 92614 USA

* Correspondence may be addressed to: Yanfeng Zhang (yanfengzhang1984@outlook.com) or Devin M. Absher (dabsher@hudsonalpha.org).

Abstract

Mapping of allelic imbalance (AI) at heterozygous loci has the potential to establish links between genetic risk for disease and biological function. Leveraging multi-omics data for AI analysis and functional annotation, we discovered a novel functional risk variant rs1047643 at 8p23 in association with SLE. This variant displays dynamic AI of chromatin accessibility and allelic expression on *FDFT1* gene in B cells with SLE. We further found a B-cell restricted super-enhancer (SE) that physically contacts with this SNP-residing locus, an interaction that also appears specifically in B cells. Quantitative analysis of open chromatin and DNA methylation profiles further demonstrated that the SE exhibits aberrant activity in B cell development with SLE. Functional studies identified that STAT3, a master factor associated with autoimmune diseases, directly regulates both the AI of risk variant and the activity of SE in cultured B cells. Our study reveals that STAT3-mediated SE activity and cis-regulatory effects of SNP rs1047643 at 8p23 locus are associated with B cell deregulation in SLE.

Introduction

Super-enhancers (SEs) are recently discovered large domains of clustered enhancers (1, 2). The extraordinary feature of SEs is the extremely high and broad enrichment of enhancer-related transcription factors (TFs), H3K4me1 and H3K27ac modifications, resulting in high capability to enhance gene expression programs (2). A large quantity of SEs show cell/tissue specificity (3), thereby they have become principal determinants of cell identity (4). Nonetheless, disease-associated SEs, in particular those exhibiting aberrant activity in autoimmune diseases, are less characterized.

Signal transducer and activator of transcription 3 (STAT3), as one of seven STAT family members, is activated by phosphorylation at tyrosine 705 (Y705) and/or at serine 727 (S727) (5). After import to the nucleus, the phospho-STAT3 (pSTAT3) modulates gene transcription by binding its target sequence (6). STAT3 has gained broad attention because it plays a key role in a variety of pathophysiological immune responses related to lymphocyte development and differentiation, and in other cellular processes of normal and tumor cells (7).

Systemic lupus erythematosus (SLE) is an autoimmune disease that is known to be associated with an array of abnormal immune cell signaling. B-cell hyperactivity in auto-antigen recognition and interaction with T-cells, which ultimately results in multi-organ damage, is central to the pathogenesis of SLE (8). Genetic factors conferring a predisposition to the development of SLE have been widely

48 characterized. Over 100 loci have been implicated in SLE by genome-wide
49 association studies (GWAS) (9, 10). Among them, several genes and/or loci are
50 potent as putative drivers of the disease. For example, genetic risk variants at the
51 promoter of *BLK* at 8p23 locus alter *BLK* transcription activity and thus contribute to
52 autoreactive B-cell responses (11). Nonetheless, the GWAS-identified genetic
53 variants together explained approximately 30% of the heritability of SLE (12, 13),
54 suggesting a requirement of further efforts to explain the missing heritability of SLE.
55 Meanwhile, there is growing evidence that genetic risk factors behave in a
56 context-dependent or cell-specific manner (11, 14). Thus, for SLE and other
57 autoimmune diseases, there is a need to identify the regulatory programs in which
58 these genetic factors impact the immune cell developmental processes.
59
60 One approach for tying genetic risk to function in the post-GWAS era (14), is a
61 measurement of allelic imbalance (AI) on two alleles at a given heterozygous locus,
62 typically at single nucleotide polymorphism (SNP). The genes and/or loci with SNPs
63 exhibiting AI could provide a strong foundation for implicating the genetic or
64 epigenetic mechanisms linked to complex traits or diseases (15, 16). As a readout of
65 AI, analyses of allele-specific chromatin accessibility and allele-specific RNA
66 expression have accumulated a wealth of interesting findings, including functional
67 cis-regulation (17, 18), genomic imprinting (19), X-chromosome inactivation or
68 escape (20). Therefore, tracking AI difference in a comparison between diseases and
69 controls may enable to uncover novel functional variants associated with complex

diseases. In this study, we describe one such strategy through integrative multi-omics analysis to discover known or novel functional variants associated with SLE, and report on the identification of a novel risk variant rs1047643 and B cell specific SE in B cells with SLE. We further demonstrate that the resultant allelic imbalanced variant and SE activity are directly controlled by STAT3, a master TF that plays a critical role in B cell development and highly associates with autoimmune diseases.

Material and methods

Reagents and Antibodies

ML115 (Cayman Chemical); S3I-201 (SML0330, Sigma); Phospho-STAT3 (Ser727) antibody (Cat No. PA5-17876, Invitrogen), Anti-Histone H3 (acetyl K27) antibody (ab4729, Abcam), H3K4me1 Recombinant Polyclonal Antibody (Cat No. 710795, Invitrogen), normal rabbit and mouse IgG (Santa Cruz Biotechnology)

Data collection

We collected a variety of functional genomics data, including ATAC-seq, RNA-seq, RRBS, Hi-C data (see details in Table S1), from the Gene Expression Omnibus (GEO) and ArrayExpress database. Meanwhile, we downloaded genotype and Epidemiological data from a SLE case-control study (accession: phs001025.v1) in Hispanic population (1,393 cases and 8,86 controls) from the dbGaP database with approval (accessed 29 Sep 2020).

92

93 **Analysis of RNA-seq and ATAC-seq data**

94 RNA-seq data were analyzed as described previously with few modifications (21). In
95 brief, raw sequencing data were mapped to the human reference genome (hg19) using
96 Hisat2 program (22) with the default setting. Aligned data were processed and
97 converted into BAM files using SAMtools program (23). The fragments per kilobase
98 of exon per million fragments mapped (FPKM) values were estimated from the
99 Cufflinks program to quantify gene expression levels.

100

101 We used a similar method described previously with several modifications (24) to
102 process the ATAC-seq data. In brief, raw sequencing data were mapped to the human
103 reference genome (hg19) using Bowtie2 program (25) with the default setting. Tag
104 per million (TPM) metric, a method commonly used for read counting normalization,
105 was used to quantitatively present the enrichment of open chromatin states across
106 regions of interest.

107

108 **Identification of allelic chromatin accessibility difference sites**

109 We used a similar approach described previously to call variants and allelic analysis
110 (20). Briefly, the deduplicated reads in BAM format were realigned and recalibrated,
111 and genetic variants were called in a multiple-sample joint manner implemented in
112 the GATK toolkit (version 3.3). We next filtered out variants as follows: (1) mapping
113 quality score < 20, (2) ≥ 3 SNPs detected within 10 bp distance, (3) variant

114 confidence/quality by depth < 2, (4) strand bias score > 50, (5) genotype score < 15
115 and (6) read depth < 8. Then, we extracted SNPs annotated from dbSNP (Build 150)
116 that were called as heterozygotes for each sample. For a reasonable comparison, those
117 heterozygous SNPs identified at least triple in both case and control samples were
118 retained. Using allelic ratio (20) as a response variable in linear regression model (see
119 below), we conducted AI analysis on chromatin accessibility for each heterozygous
120 SNP in a comparison between SLE and controls.
121 $\text{Allelic ratio} \sim \alpha + \beta * \text{disease} + \varepsilon$
122 The p-values and beta coefficients were calculated to estimate the significance of the
123 association, and the differences between cases and controls, respectively.
124

125 **Association analysis**

126 For genotype data from a SLE case-control study in Hispanic population, all typed
127 SNPs in chromosome 8 were extracted for imputation using TOPMed Imputation
128 Server (26). To test SNP rs1047643 in association with SLE, we used a method
129 described previously for univariate and haplotype analyses (27). In brief, the
130 per-allele odds ratio (OR) and 95% confidence interval (CI) for the rs1047643 was
131 estimated for SLE risk using a log-additive logistic model with covariates of
132 populations, sex and five principal components (PCs). We used the haplo.stats
133 package in R for haplotype analyses with populations, sex and five PCs as covariates.
134

Super-enhancer annotation

We downloaded whole-genome chromatin state segmentation data (core 15-state model) for 127 cell types from the Roadmap project. As Parker et al. (28) defined, we consider contiguous genomic region marked by states 6-7 (enhancer states, annotated by chromHMM) with ≥ 3 kb as SE in a cell type. Then, we extracted and annotated super-enhancers on 8p23 locus.

Analysis of eQTL data

We collected eQTL data sets from three large-scale studies, the Genotype-Tissue Expression (GTEx, v8) (29), the Haploreg v4.1 dataset (30) and the study by Westra et al. (31). By searching for the SNP rsID or the coordinate, we extracted the linked genes with query SNPs and plotted the results based on the significance and studies.

Hi-C data analysis

For in situ Hi-C dataset (Accession ID: GSE63525), we downloaded the Hi-C binary file from Rao et al. study (32) and extracted the observed long-range interactions normalized with Knight-Ruiz matrix balancing (KR) method at 10 kb resolution across the 8p23.1 region (the coordinate: chr8:11260000-11740000, hg19).

For other genome-wide Hi-C (Accession ID: GSE113405) and capture Hi-C (CHi-C) datasets (Accession ID: GSE81503 and E-MTAB-6621), we used the Hi-C Pipeline (HiCUP) (33) to truncate and align reads to the human reference genome. The deduplicated data were then processed using the Homer pipeline (34) to call the

significant chromatin interaction at 10 kb resolution. The resulting interactions were visualized using UCSC Genome Browser or Sushi package in R environment.

DNA methylation analysis

We downloaded the processed RRBS dataset of DNA methylation profiles on each CpG site from Scharer et al. report (35) , then extracted and compared CpG methylation levels on a region of interest between SLE and healthy controls.

Cell culture

GM11997 B lymphoblastic (purchased from Coriell Institute) cells were cultured in RPMI-1640 medium, supplemented with 10% FBS (Thermo Fisher Scientific), 2 mM L-glutamine and 1% penicillin-streptomycin at 37 °C with 5% CO_2. For perturbation of STAT3, B cells were plated in 12-well plates or 10 cm dishes one day prior to the experiment. Cells were then treated with S3I-201 or ML115. Cells were harvested, washed with PBS and analyzed for proper assays.

Reverse transcription qPCR

Total RNA was isolated from cells using TRIzol Reagent (Invitrogen) according to the manufacturer's protocol. 1 μg of total RNA was reverse transcribed using SuperScript III reverse transcriptase and random hexamer. One-tenth of the RT reaction was used as a template for real-time PCR using Luna Universal qPCR Master Mix (New England Biolabs) on a QuantStudi 6 system. Relative expression was

179 calculated with $2^{-\Delta\Delta Ct}$ using the average value of housekeeping gene *GAPDH*.

180

181 **Chromatin immunoprecipitation**

182 ChIP was performed as described previously. (2) Approximately 10×10^6 suspension
183 cells were harvested and in 10 ml PBS with 1% formaldehyde for 10 min at room
184 temperature, followed by adding 0.125 M glycine for 5 min. Cells were washed and
185 pelleted by centrifugation and lysed with buffer (50 mM Tris-HCl, pH 7.5, 1%
186 IGEPAL CA-630, 1 mM EDTA, 0.1% SDS, plus 1 mM PMSF) in the presence of
187 protease inhibitors and incubated on ice for 30 min. Cell lysate was sonicated to shear
188 DNA to a length of 200–600 bp. The lysates were centrifuged, and supernatant
189 transferred to new tubes. For immunoprecipitation, approximately 2×10^6 cells and
190 2-3 μg of antibodies or isotype matched IgG as control were used per ChIP and
191 incubated with supernatant at 4°C on a rotating wheel overnight. Chromatin-antibody
192 complexes were sequentially washed with low-salt buffer, high-salt buffer, LiCl
193 buffer, and TE buffer. Cross-links were reversed by addition of 100 μl of 1% SDS
194 plus 100 mM $NaHCO_3$ and by heating at 65°C overnight. Following
195 phenol/chloroform/isoamyl alcohol extraction, immunoprecipitated DNA was
196 precipitated with isopropyl alcohol and resuspended in nuclease-free water. For the
197 identification of the specific regions of interest, ~10 ng of purified DNA was
198 quantified to determine the percentage of each analyzed region against input DNA.
199 The PCR primers are shown in Table S3.

200

Statistical analysis

Data were presented as mean ± SD of three replicates unless stated otherwise. Correlation analysis was performed using Pearson's correlation coefficient. The differences were considered statistically significant at two-sided P-values less than 0.05.

Results

Multi-omics data summary

Functional genomics sequencing data sets comprising 279 samples from eleven studies were collected (Table S1). Of eleven studies, seven are SLE case-control studies with data across three immune cell types including B cells, T cells and Neutrophils (Table S2). Also included in the present study were SNP microarray data from a SLE GWAS study (n = 2,279).

Identification of SLE-associated variant showing AI at both chromatin and RNA levels

We next designed a two-stage study (Figure 1) to identify putative SLE-associated functional variants. In stage I, also termed as the discovery stage, two chromatin accessibility (ATAC-seq) data sets (Accession ID: GSE118253 and GSE71338, Table S1) comprised 49 samples were analyzed. We focused on those variants displaying difference in AI of chromatin accessibility at heterozygous SNP sites in a comparison

223 between SLE and controls (see Methods in detail). From the reciprocal validation
224 between two data sets, SNP rs1047643 was identified to show the significant AI in B
225 cells from patients with SLE, relative to controls (Figure 2A). Interestingly, in B cells
226 at different stages, the allelic preference of chromatin accessibility for this
227 SLE-associated SNP is alterable. For example, the T allele exhibits more preferential
228 chromatin accessibility in activated B cells from patients, relative to the C allele.
229 However, the direction is reversed in SLE naive B cells.
230
231 Because the rs1047643 is located in the first exon of *FDFT1* gene (Figure 3E), it
232 enables us to test the functionality of this variant at the transcriptional level.
233 Analyzing RNA-seq data (Accession ID: GSE118254), we determined the AI of RNA
234 transcripts for the rs1047643. In line with results shown above, we observed the
235 dynamic AI pattern on the transcriptional level for the rs1047643 (Figure 2B).
236 Meanwhile, this dynamic allelic expression pattern is specific during B cell
237 development with SLE (Figure 2C).
238
239 **Association with SLE risk in American Hispanic populations**
240 Because SNP rs1047643 has not been reported to be associated with the susceptibility
241 of SLE and other autoimmune diseases, we next tested the association using a dataset
242 from an SLE GWAS case-control study. Employing the univariate analysis for SNP
243 rs1047643 in samples from Hispanic populations, we identified an association of the
244 rs1047643 with SLE risk at statistical significance of adjusted $P = 0.02$ (Figure 3A),

albeit not reaching the significance after adjustment for 12 GWAS index SNPs (the top track in Figure 3E, where one SNP rs2736336 is excluded due to its multivariate alleles). Of the 12 index SNPs, indeed, one index SNP rs17807624 with the statistical significance with $P < 1.5 \times 10^{-3}$ using the univariate analysis, is the top signal to which the SNP rs1047643 is conditional. Thus, we performed haplotype analyses on these two SNPs (index SNP rs17807624 and rs1047643, Figure 3B). Compared with the reference haplotype, which carries the alleles associated with a reduced risk in two SNPs, haplotype 2, which carries the risk-associated alleles, showed a significant association (adjusted $P = 0.03$).

Functional annotation

An analysis of eQTL data derived from three independent cohorts indicated both proximal (< 200 kb) and distal (> 200 kb) regulatory potential for the SNP rs1047643 in normal B or blood cells (Figure 3D). Interestingly, besides correlated with three adjacent genes (*FDFT1*, *CTSB* and *NEIL2*), the rs1047643 is also an eQTL linked with an upstream *BLK* gene in a distance of ~300 kb, a result that is detected in two independent data sets. An analysis of RNA-seq data from two independent studies (Accession ID: GSE118254 and GSE92387, Table S1) consistently showed that expression patterns for two representative genes (*BLK* and *FDFT1*) are gradually increased in a developmental process from naive to memory B cells, in particular, the double negative memory B cell subset in patients with SLE, the pattern that is not observed in controls (Figure S1 and S2).

By searching for enhancers and other regulatory elements across 8p23 locus from a dataset of the 127 epigenomes from Roadmap, we identified a SE with a length of 7kb in the upstream of *BLK* gene in CD19+ B cells (Epigenome ID: E032, Figure 3E). An analysis of annotated enhancer elements across the 127 epigenomes showed 43 (33.9%) epigenomes had enhancers at this SE region. Comparative analysis of the enhancer length at this SE region on the 43 epigenomes further showed that this SE is specific in CD19+ B cells (Epigenome ID: E032, Figure 3C).

Analyzing Hi-C data sets from two independent studies in GM12878 cells, we observed a DNA looping between the SNP rs1047643 within FDFT1 and the SE region (Figure 3F). More importantly, in GM12878 B-lymphoblastic cells, this SE region has a wealth of long-range interactions with adjacent genes (e.g., BLK) and functional elements. In contrast, in another seven cells (Figure 3G), as well as in normal T cells (Figure S3) and nine selected tissues (Figure S4), these interactions are either much weaker or completely absent. These results indicate that the physical interaction between SNP rs1047643 and SE region, and many interactions with this SE, are specific to B-lymphocytes.

Specificity in B cells

We then hypothesized that the SE region may show aberrant activity in B cells from

289 SLE patients. To test this hypothesis, we conducted quantitative analysis on the same
290 ATAT-seq data (Accession ID: GSE118253 and GSE71338) used in stage I (see
291 Methods in detail). Comparison of SE activity in a quantitative manner between SLE
292 patients and controls indicated that the SE activity is gradually increased through B
293 cell development in SLE patients (Figure 4A-B), with a hyper-activity being observed
294 in double negative (DN) B cells in patients, relative to controls (Figure 4B-C).
295 Similarly, the rs1047643-containing promoter activity also shows up-regulation
296 towards B cell development in SLE patients (Figure 4D-E). In a comparison of B cell
297 development on activities of SE and FDFT1 promoter regions in two individuals, the
298 chromatin accessibility on both regions in an individual with SLE is increased during
299 B cell development, but remains relatively unchanged in the healthy individual
300 (Figure 4F-H).
301
302 We also quantitatively compared open chromatin states of SE and FDFT1 promoter
303 regions in resting naive B cells (Accession ID: GSE71338). Concordant with the
304 results from active B cell subsets, the open chromatin states on both regions are low
305 in non-active B cells from SLE patients, relative to healthy controls (Figure S5).
306
307 We further conducted quantitative analyses on ATAC-seq data from another two
308 independent studies in two immune cell types, T cells and neutrophils (Accession ID:
309 GSE139359 and GSE110017, Table S1). The results showed that there was no
310 marked enrichment of ATAC-seq reads on both the SE and FDFT1 promoter regions

311 in these two immune cell types for both SLE and controls (Figure S6). Collectively,
312 these results suggest a B cell specific, rs1047643-interacting SE whose activity is
313 aberrant in SLE B cell development.
314
315
316 **Hypomethylation in SLE B cells**
317 We further analyzed DNA methylation in the SE region using RRBS data in B cell
318 development in a comparison between SLE and controls (Accession ID: GSE118255,
319 Table S1). Our results show that DNA methylation levels on the SE region are
320 gradually decreased in the developmental process from resting native (rN) to memory
321 B cells in patients with SLE (Figure 5A). In contrast, there is no such obvious change
322 of DNA methylation pattern in the control group. A correlation analysis also showed
323 a marked negative correlation between open chromatin states (TPM values, also
324 presented on Figure 4E) and DNA methylation levels at the SE region in the SLE
325 group, relative to the healthy controls (Figure 5B). Together, these results reinforce
326 the aberrant activity of SE in developmental process of B-lymphocytes in patients
327 with SLE.
328
329 **STAT3 binding on both super-enhancer and rs1047643-residing regions**
330 TF-motif enrichment and binding analysis using the ENCODE TF ChIP-seq dataset
331 (v3) predicted that STAT3 may bind to both the SNP rs1047643-containing promoter
332 and SE regions (data not shown). To validate the finding, we designed two pairs of

primers (SE5 and SE3, Figure 6A) to determine the STAT3 binding on SE region and its contribution to the SE activity using STAT3, H3K4me1 and H3K27ac ChIP-qPCR assays in GM11997 cells. Under normal culture conditions, we validated that pSTAT3, H3K4me1 and H3K27ac modifications are remarkably enriched on the SE region in B-lymphoblastic cells, relative to IgG mock controls (Figure 6A, 6E and 6F). We then conducted both the inhibition and activation of STAT3 DNA binding activity using two small molecules. In B-lymphoblastic cells challenged with S3I-201, a STAT3 DNA binding inhibitor, both the DNA binding of STAT3 on SE region and the SE activity are significantly reduced (Figure 6A), relative to control. In GM11997 cells treated with ML115, a selective activator of STAT3 (36), both the STAT3 DNA binding capability on SE region and the SE activity are significantly increased (Figure 6E), relative to controls. These results together demonstrate that STAT3 directly modulates the SE activity.

We next tested whether the STAT3 might also regulate the rs1047643-residing regions. Using allelic qPCR assay, we confirmed that genomic DNA in the GM11997 cells carries a heterozygous variant for the SNP rs1047643 (Figure S7), enabling the AI analysis in this cell model. In GM11997 cells treated with the STAT3 inhibitor S3I-201, STAT3 binding on the risk allele T is significantly reduced, relative to the rs1049643-C allele (Figure 6B). Concordantly, the expression level on the rs1049643-T allele is also declined after treatment with S3I-201 for 24 hours, relative to the C allele (Figure 6C). Conversely, we observed an increase of both STAT3

355 DNA binding and expression at the rs1049643-T allele in cells stimulated with the
356 STAT3 activator ML115 (Figure 6F-G). These results collectively suggest that the
357 risk rs1049643-T allele is preferentially bound by STAT3 in B cells.
358
359 We also determined RNA expression of BLK and FDFT1, two representative genes
360 that correlate with the risk rs1047643. The expression levels of both genes are
361 decreased with the treatment of S3I-201 (Figure 6D), and up-regulated with the
362 STAT3 activator ML115 (Figure 6H). These results suggest the STAT3-binding risk
363 allele T is associated with increased expression of *BLK* and *FDFT1*.
364
365

366 ## Discussion

367 In the present study, by integrating a variety of functional genomic data, we
368 performed AI analysis to uncover novel functional promising variants and their
369 regulatory targets in association with SLE. Of note, the diversity of genomic data
370 types from this comprehensive data collection for autoimmune diseases allowed us to
371 develop an approach not used before for accessing the role of variants in SLE disease
372 activity.
373
374 One of the most significant findings is the identification of a novel risk variant
375 rs1047643. The association study shows that the rs1049643-T is a risk allele for SLE.
376 Our AI analyses indicate that the rs1049643-T allele resides in more open chromatin

state and has higher expression in SLE memory B cell subsets, relative to the C allele. Functional study further provides evidence that the rs1049643-T allele is preferentially bound by STAT3. The SNP rs1047643 is also an eQTL linked with both proximal and distal genes, including *BLK*, the gene that plays a critical role in B lymphocyte development (37). These results demonstrate that this novel SLE-associated risk rs1047643 whose functionality is mediated by STAT3, may play a role in allele-specific control of adjacent genes at 8p23 locus in B cells. Despite no report for association with other autoimmune diseases, this SNP has been associated with multiple myeloma (38) and follicular lymphoma (39), two malignant diseases whose pathogenesis is partially associated with the dysfunction of B cells. Specifically, hyperactive STAT3 has been reported to be associated with poor survival in both diseases (40, 41). Therefore, our findings may provide a clue for genetic and mechanical studies on those B cell associated diseases.

Another intriguing finding in this study is the identification of an aberrant activity of a SE in lupus B cell subsets, particularly the hyperactivity in memory B cells. In contrast, there is no enhancer activity in other immune cells (T cells and neutrophils analyzed in this study) in patients with SLE. We also demonstrate that the aberrant activity of the SE can be mediated by STAT3. Some studies have consistently reported a critical role of STAT3 in the B cell maturation, differentiation, as well as the autoimmunity (42, 43). These reports further support the significance of STAT3-mediated SE aberration in B cells with SLE.

Several studies have highlighted the 8p23 locus as a major SLE susceptibility region (44). Our study further expands the significance at this locus. We speculate that the 8p23 locus may play functional roles in B cell development in both genetic and epigenetic fashions. Besides the SNP rs1047643 discovered in the present study, there are 13 SLE-associated GWAS leading SNPs reported in this locus. Of 13 SNPs, six SNPs (Figure 3E) directly sit in the SE region, suggesting these risk variants may play roles in a genetic interaction way. For example, our study and others together suggest that there are a few cis-eQTLs linked with transcriptional levels of BLK (11, 44). Epigenetically, the SLE-associated SE has physical interactions with adjacent genes, including *BLK* and *FDFT1*, and the risk rs1047643-residing region. This indicates a potentially complex role of the variant rs1047643 for broad regulation by physically contacting the SE. Thus, our data provide new insights into the molecular mechanisms by merging genetic susceptibility with epigenetic impacts on gene expression for autoimmune diseases.

The *FDFT1* is a gene encoding for squalene synthase, the enzyme that catalyzes the early step in the cholesterol biosynthetic pathway (45). Previous studies have shown dyslipidemia, with elevations in total cholesterol, low-density lipoprotein, triglyceride levels in patients with lupus (46), especially in the active disease. Our multi-omics data indicate that the SNP rs1047643-linked FDFT1 is aberrantly activated in B cell development in SLE patients, thereby providing an insight into the genetic

implication of lipid metabolism for autoimmune diseases.

The limitations of this study include, due to the presence of six SLE GWAS tagging SNPs in SE region, we are unclear how they genetically influence the SE activity during B cell development. Second, it remains unclear how the AI pattern occurs in naive B cells with lupus. The C allele shows more open chromatin state in SLE naive B cells, this can't be explained by STAT3 allelic DNA binding at the T allele. This implies that some other factors may also contribute to this dynamic AI pattern.

In conclusion, we identified a novel functional variant and B cell specific SE in association with the SLE pathogenesis, both mediated by STAT3, and influencing their gene targets. This insight into the mechanism by which manipulation of STAT3 affects the SE activity and its associated gene expression in B cells may have implications for future drug development in autoimmunity.

Author contributions

Y.Z. conceived and designed the study, collected and analyzed the data, conducted the experiments, wrote the manuscript. D.A. contributed materials and data, and assisted in data analysis, interpreted the data and edited the manuscript. All authors read and approved the final manuscript.

Declaration of interests

The authors declare no competing financial interests.

Funding

This study was supported by the HudsonAlpha Institute Fund. The funders had no role in study design, data collection and analysis, decision to publish, or preparation of the manuscript.

Acknowledgments

We thank Dr. Le Su for insightful suggestions, technical discussions and critical reading of the manuscript. This study was supported by the HudsonAlpha institutional funds. The funders had no role in study design, data collection and analysis, decision to publish or preparation of the manuscript.

References

1. Parker SCJ, Stitzel ML, Taylor DL, Orozco JM, Erdos MR, Akiyama JA, et al. Chromatin stretch enhancer states drive cell-specific gene regulation and harbor human disease risk variants. Proceedings of the National Academy of Sciences. 2013;110(44):17921-6.

2. Whyte WA, Orlando DA, Hnisz D, Abraham BJ, Lin CY, Kagey MH, et al. Master Transcription Factors and Mediator Establish Super-Enhancers at Key Cell Identity Genes. Cell. 2013;153(2):307-19.

3. Vahedi G, Kanno Y, Furumoto Y, Jiang K, Parker SCJ, Erdos MR, et al. Super-enhancers delineate disease-associated regulatory nodes in T cells. Nature. 2015;520(7548):558-62.

4. Hnisz D, Abraham Brian J, Lee Tong I, Lau A, Saint-André V, Sigova Alla A, et al. Super-Enhancers in the Control of Cell Identity and Disease. Cell. 2013;155(4):934-47.

5. Decker T, Kovarik P. Serine phosphorylation of STATs. Oncogene. 2000;19(21):2628-37.

6. Levy DE, Darnell JE. STATs: transcriptional control and biological impact. Nature Reviews Molecular Cell Biology. 2002;3(9):651-62.

7. Yu H, Pardoll D, Jove R. STATs in cancer inflammation and immunity: a leading role for STAT3. Nature Reviews Cancer. 2009;9(11):798-809.

8. Rahman A, Isenberg DA. Systemic Lupus Erythematosus. New England Journal of Medicine. 2008;358(9):929-39.

9. Catalina MD, Owen KA, Labonte AC, Grammer AC, Lipsky PE. The pathogenesis of systemic lupus erythematosus: Harnessing big data to understand the molecular basis of lupus. Journal of Autoimmunity. 2020;110:102359.

10. Yin X, Kim K, Suetsugu H, Bang S-Y, Wen L, Koido M, et al. Meta-analysis of 208370 East Asians identifies 113 susceptibility loci for systemic lupus erythematosus. Annals of the Rheumatic Diseases. 2021;80(5):632-40.

11. Guthridge JM, Lu R, Sun H, Sun C, Wiley GB, Dominguez N, et al. Two functional lupus-associated BLK promoter variants control cell-type- and

487 developmental-stage-specific transcription. American journal of human genetics.
488 2014;94(4):586-98.
489 12. Sun C, Molineros JE, Looger LL, Zhou X-j, Kim K, Okada Y, et al. High-density
490 genotyping of immune-related loci identifies new SLE risk variants in individuals
491 with Asian ancestry. Nature Genetics. 2016;48(3):323-30.
492 13. Morris DL, Sheng Y, Zhang Y, Wang Y-F, Zhu Z, Tombleson P, et al.
493 Genome-wide association meta-analysis in Chinese and European individuals
494 identifies ten new loci associated with systemic lupus erythematosus. Nature Genetics.
495 2016;48(8):940-6.
496 14. Gallagher MD, Chen-Plotkin AS. The Post-GWAS Era: From Association to
497 Function. American journal of human genetics. 2018;102(5):717-30.
498 15. Pastinen T, Hudson TJ. Cis-Acting Regulatory Variation in the Human Genome.
499 Science. 2004;306(5696):647-50.
500 16. Yan H, Yuan W, Velculescu VE, Vogelstein B, Kinzler KW. Allelic variation in
501 human gene expression. Science. 2002;297(5584):1143.
502 17. Li Q, Seo JH, Stranger B, McKenna A, Pe'er I, Laframboise T, et al. Integrative
503 eQTL-based analyses reveal the biology of breast cancer risk loci. Cell.
504 2013;152(3):633-41.
505 18. Zhang S, Zhang H, Zhou Y, Qiao M, Zhao S, Kozlova A, et al. Allele-specific
506 open chromatin in human iPSC neurons elucidates functional disease variants.
507 Science. 2020;369(6503):561-5.
508 19. Pollard KS, Serre D, Wang X, Tao H, Grundberg E, Hudson TJ, et al. A

509 genome-wide approach to identifying novel-imprinted genes. Human genetics.
510 2008;122(6):625-34.
511 20. Zhang Y, Li X, Gibson A, Edberg J, Kimberly RP, Absher DM. Skewed allelic
512 expression on X chromosome associated with aberrant expression of XIST on
513 systemic lupus erythematosus lymphocytes. Human molecular genetics.
514 2020;29(15):2523-34.
515 21. Zhang Y, Wagner EK, Guo X, May I, Cai Q, Zheng W, et al. Long intergenic
516 non-coding RNA expression signature in human breast cancer. Scientific reports.
517 2016;6:37821.
518 22. Kim D, Paggi JM, Park C, Bennett C, Salzberg SL. Graph-based genome
519 alignment and genotyping with HISAT2 and HISAT-genotype. Nature biotechnology.
520 2019;37(8):907-15.
521 23. Li H, Handsaker B, Wysoker A, Fennell T, Ruan J, Homer N, et al. The
522 Sequence Alignment/Map format and SAMtools. Bioinformatics.
523 2009;25(16):2078-9.
524 24. Zhang Y, Delahanty R, Guo X, Zheng W, Long J. Integrative genomic analysis
525 reveals functional diversification of APOBEC gene family in breast cancer. Human
526 Genomics. 2015;9(1):34.
527 25. Langmead B, Salzberg SL. Fast gapped-read alignment with Bowtie 2. Nature
528 methods. 2012;9(4):357-9.
529 26. Das S, Forer L, Schonherr S, Sidore C, Locke AE, Kwong A, et al.
530 Next-generation genotype imputation service and methods. Nat Genet.

2016;48(10):1284-7.

27. Shi J, Zhang Y, Zheng W, Michailidou K, Ghoussaini M, Bolla MK, et al. Fine-scale mapping of 8q24 locus identifies multiple independent risk variants for breast cancer. Int J Cancer. 2016;139(6):1303-17.

28. Parker SC, Stitzel ML, Taylor DL, Orozco JM, Erdos MR, Akiyama JA, et al. Chromatin stretch enhancer states drive cell-specific gene regulation and harbor human disease risk variants. Proceedings of the National Academy of Sciences of the United States of America. 2013;110(44):17921-6.

29. Consortium GT, Laboratory DA, Coordinating Center -Analysis Working G, Statistical Methods groups-Analysis Working G, Enhancing Gg, Fund NIHC, et al. Genetic effects on gene expression across human tissues. Nature. 2017;550(7675):204-13.

30. Ward LD, Kellis M. HaploReg v4: systematic mining of putative causal variants, cell types, regulators and target genes for human complex traits and disease. Nucleic acids research. 2016;44(D1):D877-81.

31. Westra H-J, Peters MJ, Esko T, Yaghootkar H, Schurmann C, Kettunen J, et al. Systematic identification of trans eQTLs as putative drivers of known disease associations. Nature Genetics. 2013;45(10):1238-43.

32. Rao Suhas SP, Huntley Miriam H, Durand Neva C, Stamenova Elena K, Bochkov Ivan D, Robinson James T, et al. A 3D Map of the Human Genome at Kilobase Resolution Reveals Principles of Chromatin Looping. Cell. 2014;159(7):1665-80.

553 33. Wingett S, Ewels P, Furlan-Magaril M, Nagano T, Schoenfelder S, Fraser P, et al.
554 HiCUP: pipeline for mapping and processing Hi-C data. F1000Research.
555 2015;4(1310).
556 34. Heinz S, Benner C, Spann N, Bertolino E, Lin YC, Laslo P, et al. Simple
557 Combinations of Lineage-Determining Transcription Factors Prime
558 cis-Regulatory Elements Required for Macrophage and B Cell Identities.
559 Molecular Cell. 2010;38(4):576-89.
560 35. Scharer CD, Blalock EL, Mi T, Barwick BG, Jenks SA, Deguchi T, et al.
561 Epigenetic programming underpins B cell dysfunction in human SLE. Nature
562 Immunology. 2019;20(8):1071-82.
563 36. Madoux F, Koenig M, Nelson E, Chowdhury S, Cameron M, Mercer B, et al.
564 Modulators of STAT Transcription Factors for the Targeted Therapy of Cancer
565 (STAT3 Activators). Bethesda: National Center for Biotechnology Information; 2010.
566 37. Saijo K, Schmedt C, Su Ih, Karasuyama H, Lowell CA, Reth M, et al. Essential
567 role of Src-family protein tyrosine kinases in NF-κB activation during B cell
568 development. Nature Immunology. 2003;4(3):274-9.
569 38. Van Ness B, Ramos C, Haznadar M, Hoering A, Haessler J, Crowley J, et al.
570 Genomic variation in myeloma: design, content, and initial application of the Bank
571 On A Cure SNP Panel to detect associations with progression-free survival. BMC
572 medicine. 2008;6:26.
573 39. Skibola CF, Bracci PM, Halperin E, Nieters A, Hubbard A, Paynter RA, et al.
574 Polymorphisms in the Estrogen Receptor 1 and Vitamin C and Matrix

575 Metalloproteinase Gene Families Are Associated with Susceptibility to Lymphoma.
576 PLOS ONE. 2008;3(7):e2816.
577 40. Huang X, Meng B, Iqbal J, Ding BB, Perry AM, Cao W, et al. Activation of the
578 STAT3 signaling pathway is associated with poor survival in diffuse large B-cell
579 lymphoma treated with R-CHOP. Journal of clinical oncology. 2013;31(36):4520-8.
580 41. Jung S-H, Ahn S-Y, Choi H-W, Shin M-G, Lee S-S, Yang D-H, et al. STAT3
581 expression is associated with poor survival in non-elderly adult patients with newly
582 diagnosed multiple myeloma. Blood Res. 2017;52(4):293-9.
583 42. Avery DT, Deenick EK, Ma CS, Suryani S, Simpson N, Chew GY, et al. B cell–
584 intrinsic signaling through IL-21 receptor and STAT3 is required for establishing
585 long-lived antibody responses in humans. Journal of Experimental Medicine.
586 2010;207(1):155-71.
587 43. Ding C, Chen X, Dascani P, Hu X, Bolli R, Zhang H-g, et al. STAT3 Signaling in
588 B Cells Is Critical for Germinal Center Maintenance and Contributes to the
589 Pathogenesis of Murine Models of Lupus. The Journal of Immunology.
590 2016;196(11):4477-86.
591 44. Demirci FY, Wang X, Morris DL, Feingold E, Bernatsky S, Pineau C, et al.
592 Multiple signals at the extended 8p23 locus are associated with susceptibility to
593 systemic lupus erythematosus. Journal of Medical Genetics. 2017;54(6):381-9.
594 45. Tozawa R-i, Ishibashi S, Osuga J-i, Yagyu H, Oka T, Chen Z, et al. Embryonic
595 Lethality and Defective Neural Tube Closure in Mice Lacking Squalene Synthase.
596 Journal of Biological Chemistry. 1999;274(43):30843-8.

46. Tisseverasinghe A, Lim S, Greenwood C, Urowitz M, Gladman D, Fortin PR. Association between serum total cholesterol level and renal outcome in systemic lupus erythematosus. Arthritis & Rheumatism. 2006;54(7):2211-9.

Figure legends

Figure 1. Schematic of the study design. On the basis of the functional genomic data feature, a two-stage study was designed. Summary of data sets are available in Table S1 and S2.

Figure 2. **Change of allelic chromatin accessibility and expression in B cell subtypes from SLE patients and controls.** (A) Forest plot showing AI of allelic chromatin state of SNP rs1047643 in both resting naive (rN) and activated (Non-rN) B cells in patients of SLE compared with healthy controls. The plot in the right panel displays the 95% of confidence interval of beta-value. (B-C) Boxplots showing allelic expression of SNP rs1047643 in both rN and activated B cells in patients with SLE as compared with healthy individuals. All raw data are available in Figure 2—source data 1.

Figure 3. Association analysis and functional prediction of SNP rs1047643. (A) Association results for the SNP rs1047643 with SLE risk in single marker analyses. MAF, minor allele frequency; OR, odds ratio; CI, confidence interval. (B) Haplotype

analyses of the two SNPs (SNP1: GWAS indexed SNP rs17807624; SNP2: rs1047643) in relation to SLE risk. Baseline (the reference haplotype) represents the alleles associated with a reduced risk in two SNPs. (C) Barplot showing the genomic length of chromHMM-annotated enhancer state on the super-enhancer region (blue highlighted in 3C) in 43 epigenomes. (D) Plot shows the eQTL result of SNP rs1047643 in whole blood or B cells from three databases (shown in y-axis). (E) Genomic annotations of the SNP rs1047643. The three tracks show locations of 13 GWAS index SNP, gene annotation and 15-state chromatin segments in CD19+ B cells at 8p23 locus, respectively. Vertical blue and purple lines, represents the location of super-enhancer and SNP rs1047643, respectively. (F) Long-range interaction between a super-enhancer and SNP rs1047643. The two tracks show chromatin interactions from two independent studies using whole-genome Hi-C and capture Hi-C technologies, respectively. Orange curves show the interactions between the super-enhancer and the SNP rs1047643. (G) Heatmaps showing the 3D DNA interactions at 8p23.1 locus in eight cell lines. The rectangle represents interactions between the super-enhancer and the SNP rs1047643. All raw data are available in Figure 3—source data 1.

Figure 4. Aberration of super-enhancer and *FDFT1* promoter region in B cell subtypes from SLE patients. (A) Empirical cumulative distribution of TPM values per 50-bp window across the 7kb SE region in B cell subsets for disease and control groups. (B) Plots showing the TPM values at the third quartile (Q3) across B cell

641 subtypes as a comparison between SLE and controls. (C) Empirical cumulative
642 distribution of TPM values on the SE region (same as shown in A) in a comparison
643 between two groups across four B cell subtypes. (D) Boxplots showing the TPM
644 values per 50-bp window at the *FDFT1* promoter region in B cell subtypes for SLE
645 and controls. The black lines and grey areas represent the linear regression results
646 towards the B cell development from T3 to DN stages, and 95% of CI. (E) Plots
647 showing the correlation between super-enhancer and *FDFT1* promoter regions based
648 on mean TPM values with respect to B cell subtypes in SLE and controls. (F) Wiggle
649 plot showing the enrichment of open chromatin states at 8p23.1 locus in B cell
650 subtypes for two individuals (a healthy individual at upper panel, and a patient with
651 SLE at lower panel). Purple and green vertical lines represent the locations for
652 super-enhancer and *FDFT1* promoter, respectively. Quantitative comparison of
653 chromatin accessibility states in SE (G) and *FDFT1* promoter regions (H) with
654 respect to B cell subtypes. All raw data are available in Figure 4—source data 1.
655
656 **Figure 5. Hypomethylation in super-enhancer region in B cell subtypes from**
657 **SLE patients.** (A) Boxplots showing the CpG methylation levels per 50-bp window
658 in 7kb SE region in B cell subtypes for SLE and control groups. The black and red
659 lines represent the linear regression results towards the B cell development from rN to
660 DN stages for SLE and controls, respectively. (B) Plots showing the correlation
661 between TPM values (y-axis) and DNA methylation levels (x-axis) averaged over
662 each B cell type in SLE and controls. All raw data are available in Figure 5—source

663 data 1.

664

665 **Figure 6. Contribution of STAT3 modulates the enhancer activity and**

666 **SNP-residing locus in cultured GM11997 cells.** (A) ChIP-qPCR for H3K27ac (left

667 lower panel), H3K4me1 (middle lower panel) and pSTAT3 (right) at 8p23

668 super-enhancer region following 40 μM S3I-201 treatment for 24h. Left upper panel:

669 UCSC genome browser showing the location of two pairs of qPCR primers (SE5 and

670 SE3) on the SE region (yellow). Two tracks shown below are the enrichment of

671 H3K27ac and H3K4me1 across the SE region. (B) Allelic ChIP-qPCR for pSTAT3

672 binding and (C) allelic RT-qPCR on SNP rs1047643 (T vs C alleles) following 40

673 μM S3I-201 treatment for 24h. (D) RT-qPCR with RNA from B-lymphoblastic cells

674 that have been challenged with S3I-201 for 24h as indicated. The fold changes for the

675 rs1047643-associated *BLK* and *FDFT1* genes in response to different concentrations

676 of S3I-201 compared to vehicle (0.1% DMSO) as control, which was set as 1 in all

677 cases, are presented. (E) ChIP-qPCR for H3K27ac (left), and pSTAT3 (right) at 8p23

678 super-enhancer region following 100 nM ML115 treatment for 6h. (F) Allelic

679 ChIP-qPCR for pSTAT3 binding and (G) allelic RT-qPCR on SNP rs1047643 (T vs

680 C alleles) following 100 nM ML115 treatment for 6h. (H) RT-qPCR with RNA from

681 B-lymphoblastic cells that have been challenged with ML115 for 6h as indicated. The

682 fold changes for the rs1047643-associated *BLK* and *FDFT1* genes in response to

683 different concentrations of ML115 compared to vehicle (0.1% DMSO) as control,

684 which was set as 1 in all cases, are presented. NS, not significance; *, $P < 0.05$; **, P

685 < 0.01; ***, $P < 0.005$.

686

687

688 ## Supplementary data

689 **Table S1. Summary of data sets used in the study.** Functional genomics data sets,
690 including ATAC-seq, RNA-seq and RRBS-seq data sets from seven SLE case-control
691 studies (Table S2), and Hi-C data sets in multiple cell lines, and a SNP microarray
692 data set from a lupus GWAS study.

693

694 **Table S2. List of data sets from seven SLE case-control studies.**

695

696 **Table S3: List of primers used in this study.**

697

698 **Figure S1 Expression pattern of FDFT1 and BLK across B cell subtypes in a**
699 **comparison from a case-control study.** Comparison of FDFT1 (A) and BLK (B)
700 expression profiles in B cell subtypes from patients with SLE and healthy individuals
701 (Accession ID: GSE118254).

702

703 **Figure S2 Expression pattern of FDFT1 and BLK across B cell subtypes in a**
704 **comparison between patients with SLE and healthy controls.** Comparison of
705 FDFT1 (A) and BLK (B) expression profiles in B cell subtypes from a case-control
706 study (Accession ID: GSE92387).

Figure S3 Chromatin interactions with *FDFT1* promoter region (marked in green arrow) on 8p23 locus from CHi-C data with duplicates in two types of normal T cells. Orange arrow represents the location of super-enhancer identified in this study.

Figure S4 Heatmaps of Long-range chromatin interactions from Hi-C data in 8p23 locus at 10 kb (or 20 kb) resolution in a panel of human tissues from the 3D Genome Browser. The circles shown on heatmaps are the interaction score between SNP rs1047643 and SE region.

Figure S5 Aberration of super-enhancer in resting naive B cell subtypes from SLE patients in relation to healthy controls. (A) Wiggle plot showing the enrichment of open chromatin states at 8p23.1 locus in resting native B cells from eight individuals. Blue and purple vertical lines represent the locations of SE and *FDFT1* promoter, respectively. (B-C) Quantitative comparison of chromatin accessibility states in the SE and FDFT1 promoter regions in naive B cells in a comparison between SLE and controls.

Figure S6 No super-enhancer activity in T and neutrophils from SLE patients and controls. (A-B) Empirical cumulative distribution of TPM values per 50-bp window and enrichment of ATAC-seq reads (TPM value) across the SE region in neutrophil cell subsets from SLE patients and controls. (C-D) Empirical cumulative

729 distribution of TPM values per 50-bp window and enrichment of ATAC-seq reads
730 (TPM value) across the SE region in two T cell subsets from SLE patients. (E)
731 Wiggle plot showing the enrichment of open chromatin states at 8p23.1 locus in
732 neutrophils and T cells. Blue and purple vertical lines represent the locations of SE
733 and *FDFT1* promoter, respectively.
734
735 **Figure S7 Genotyping of SNP rs1047643 in GM11997 genomic DNA using allelic**
736 **qPCR analysis.** Amplification plots are presented for two alleles.
737
738 **Figure 2—source data 1**
739 **Source files for presenting results in Figure 2.**
740 This zip archive contains all source data used for the quantitative analyses shown in
741 Fig. 2.
742
743 **Figure 3—source data 1**
744 **Source files for presenting results in Figure 3.**
745 This zip archive contains all source data used for the quantitative analyses shown in
746 Fig. 3.
747
748 **Figure 4—source data 1**
749 This txt file contains source data used for the quantitative analyses shown in Fig. 4.
750

751 **Figure 5—source data 1**

752 This txt file contains source data used for the quantitative analyses shown in Fig. 5.

753

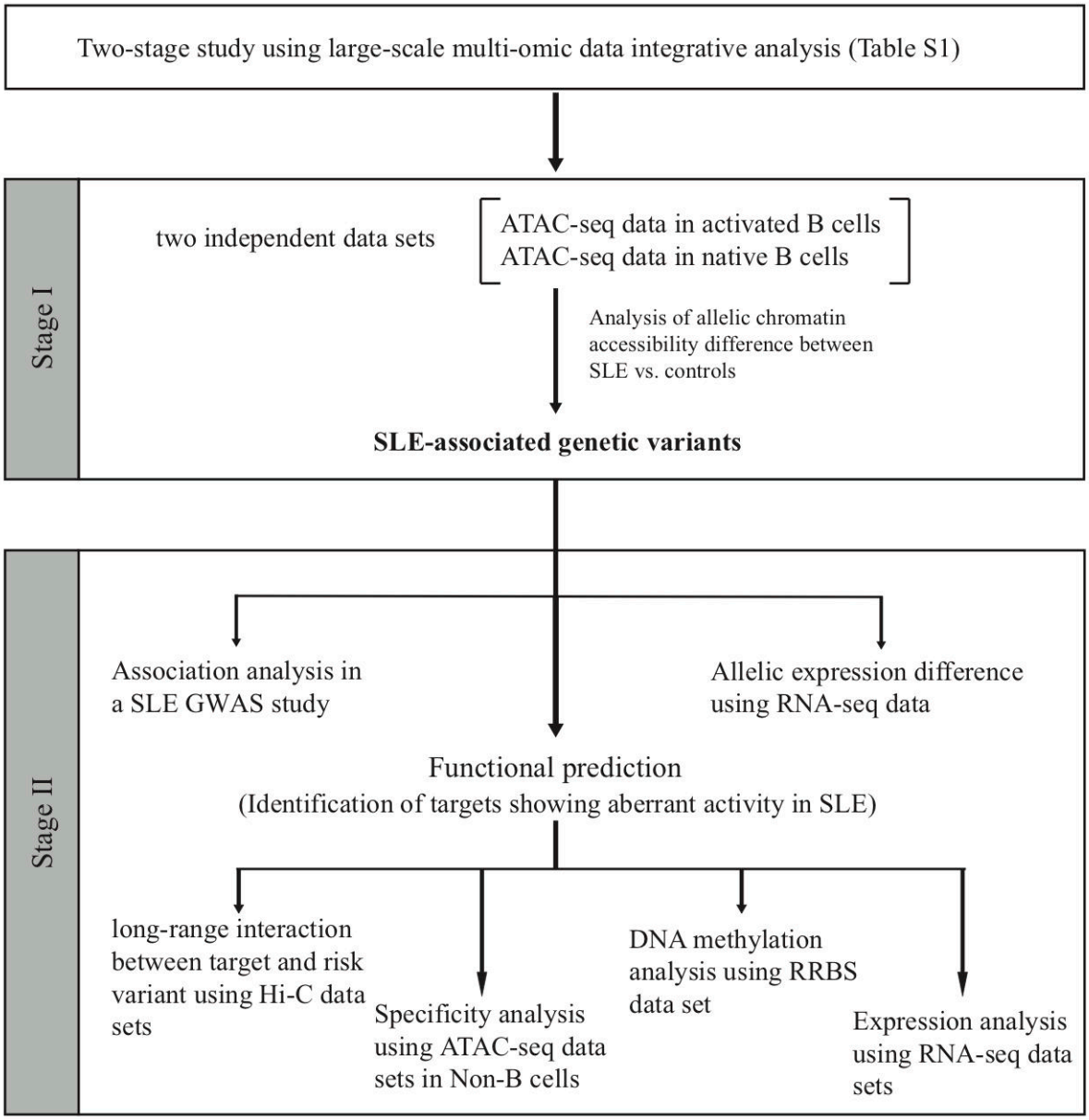

A

Study	rs1047643	SLE (AR)	CNTL (AR)	P.value	Beta
Non-rN B cells	T vs. C	0.59	0.45	5.5e-03	0.14
rN B cells	C vs. T	0.62	0.48	4.6e-02	0.14
Summary				**2.4e-03**	**0.14**

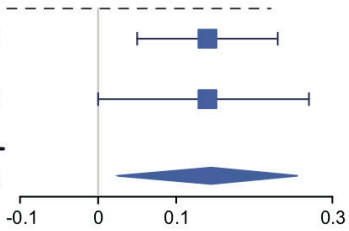

B

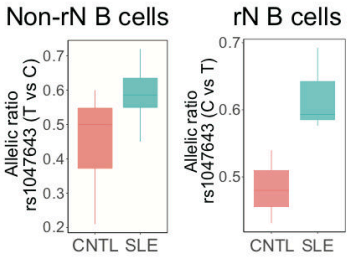

C

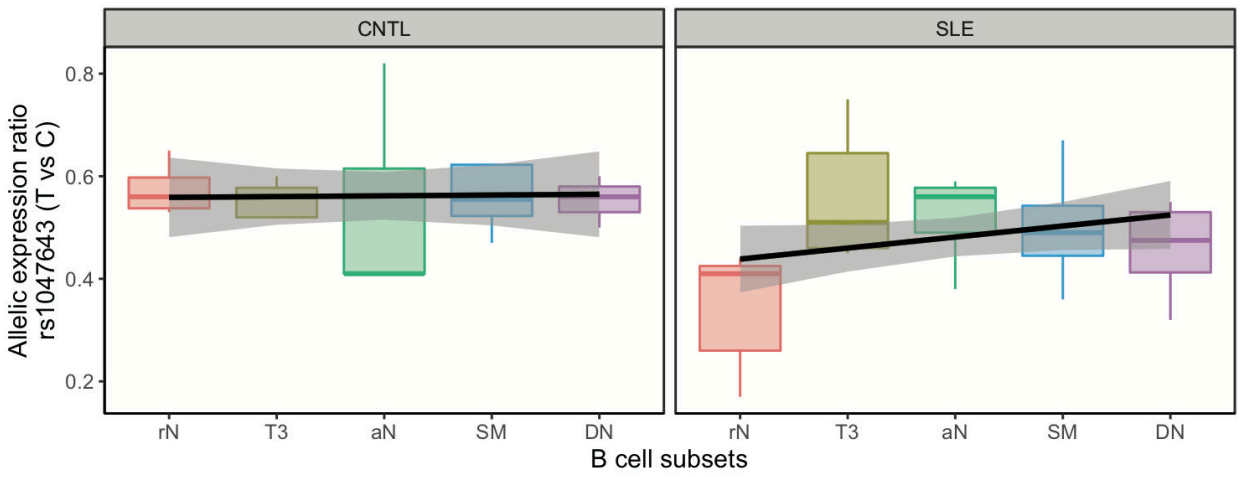

A

SNP	Alleles	MAF	Imputation score	Univariate analysis		Conditional analysis	
				OR (95% CI)	Adjusted P	OR (95% CI)	Adjusted P
rs1047643	T/C	0.08	0.99	0.77 (0.54 - 0.99)	0.023	0.93 (0.68 - 1.18)	0.57

B

Haplotypes	SNP 1	SNP 2	Frequency	OR (95% CI)	Adjusted P
	C/T	T/C			
Baseline	C	C	0.052	reference	-
Haplo.1	C	T	0.515	1.11 (0.79 - 1.54)	0.55
Haplo.2	T	T	0.431	1.44 (1.04 - 2.0)	0.03
Haplo.3	T	C	0.002	0.77 (0.07 - 8.5)	0.83

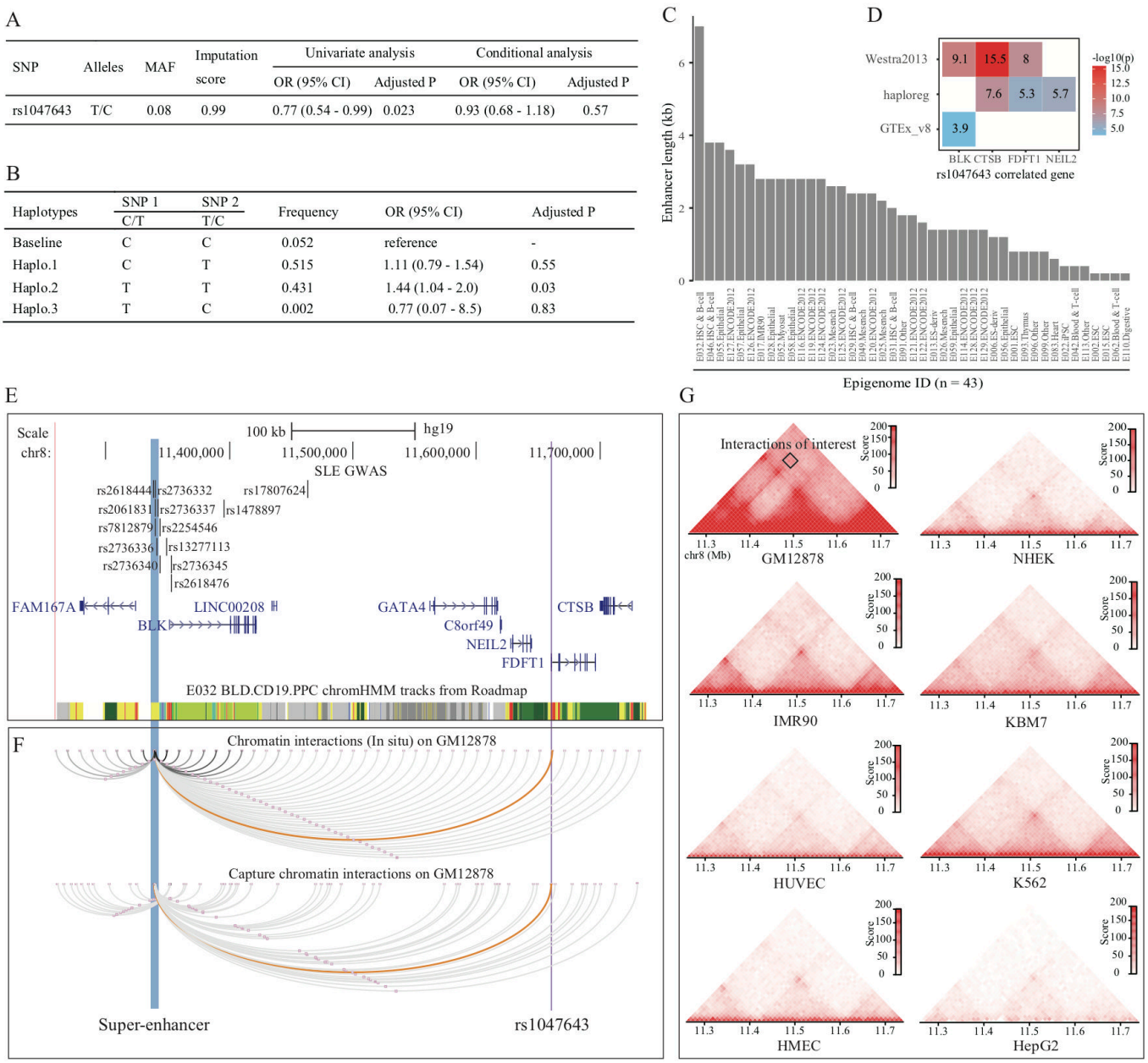

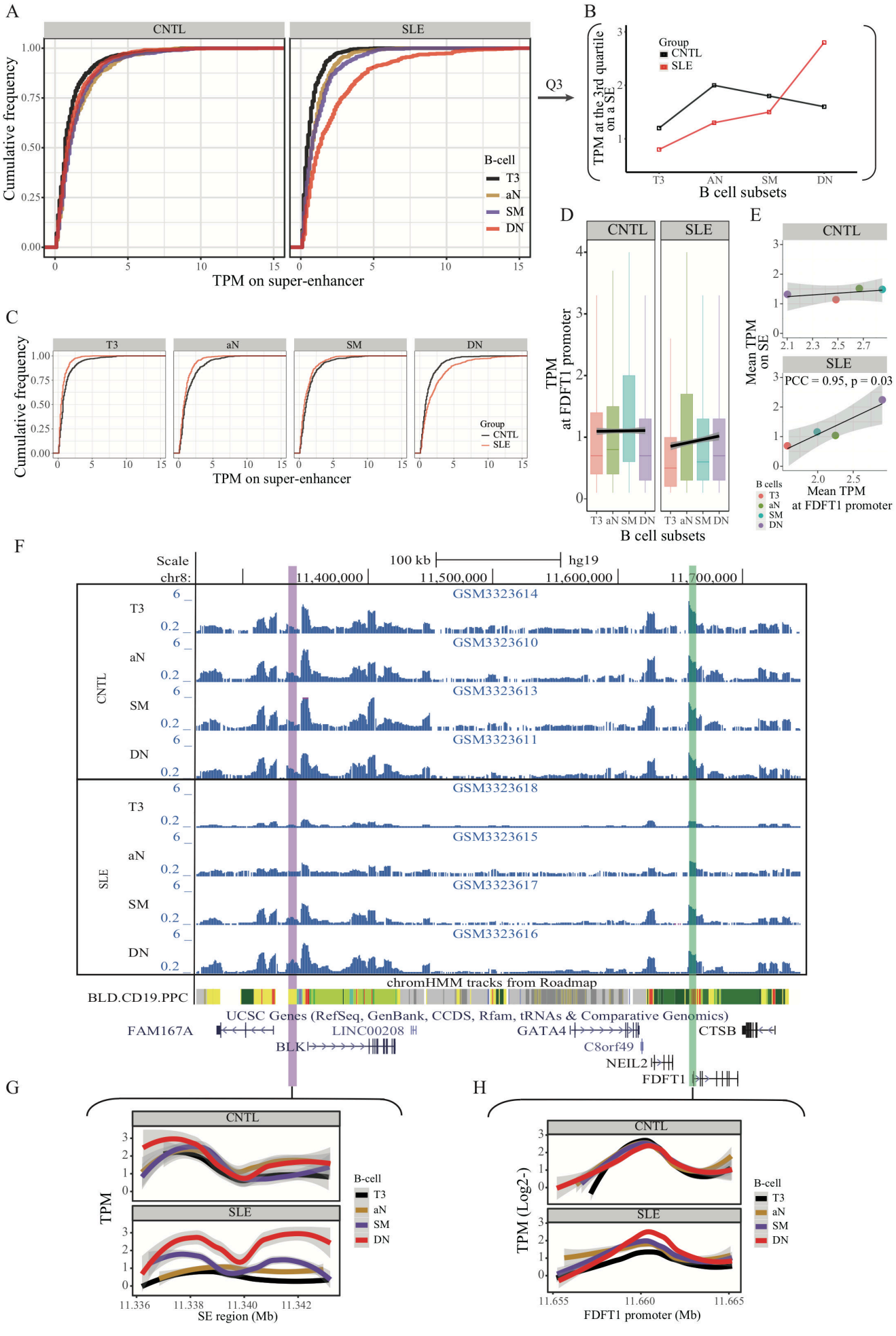

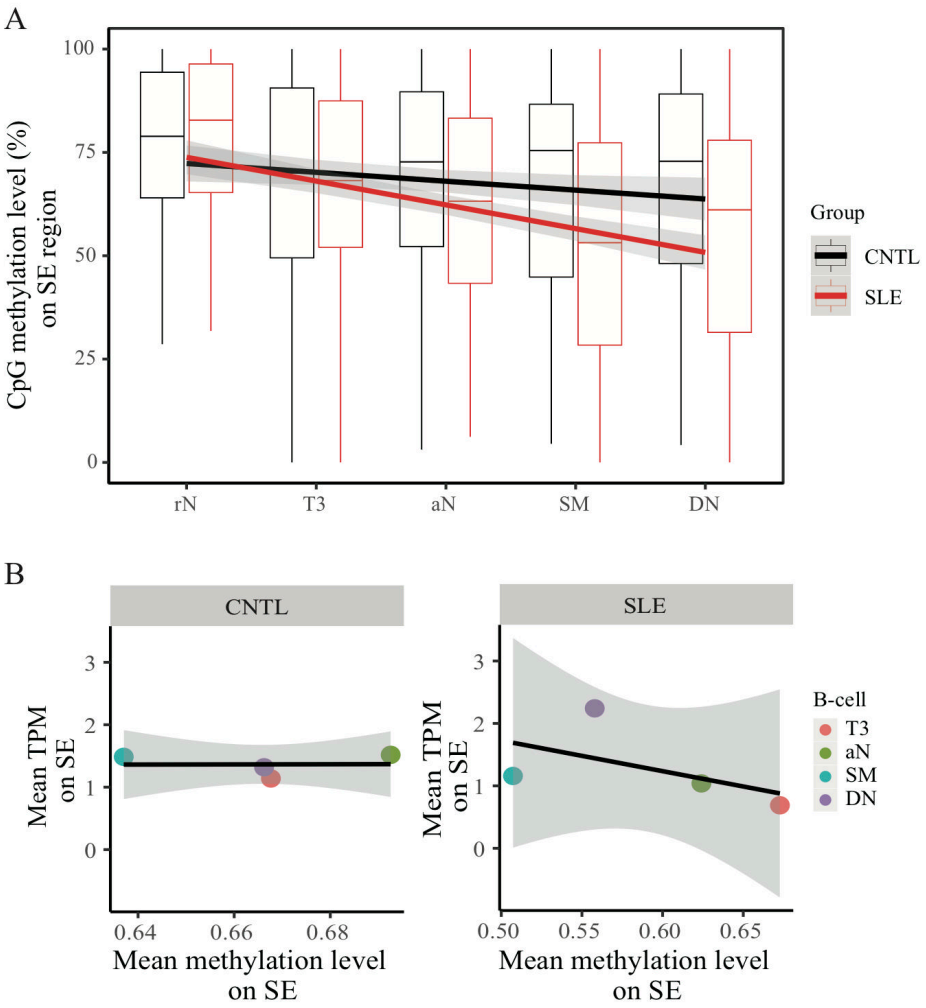

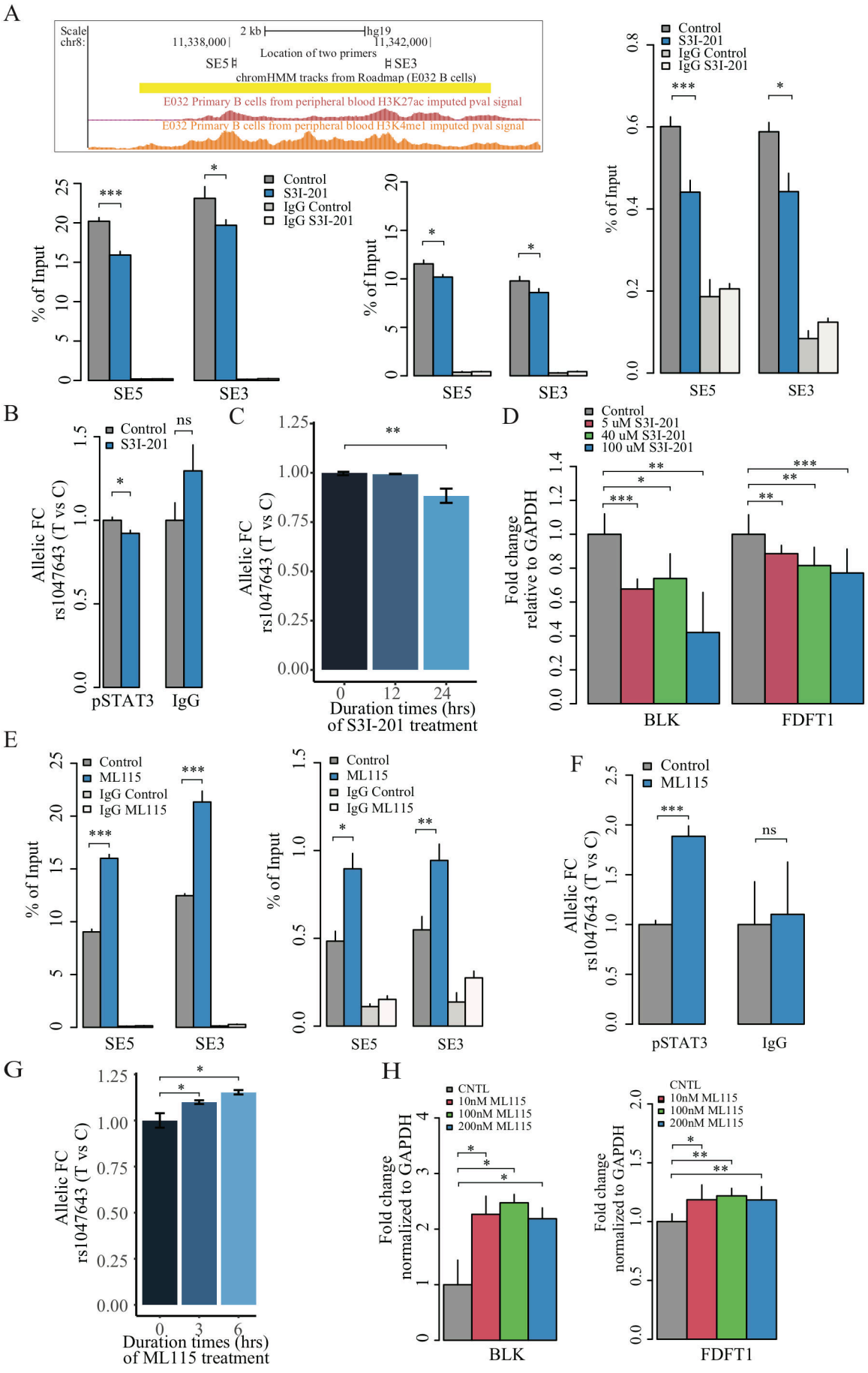

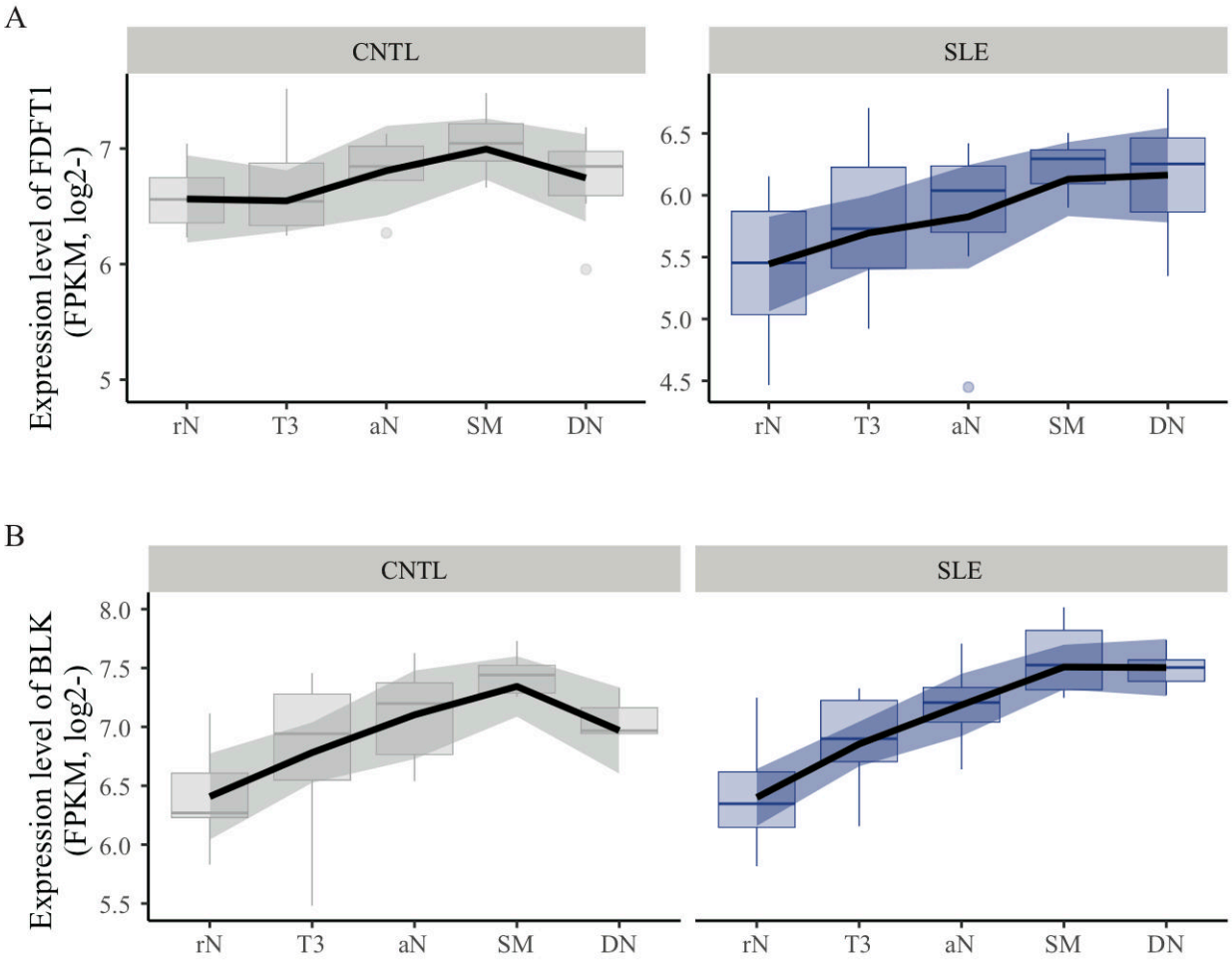

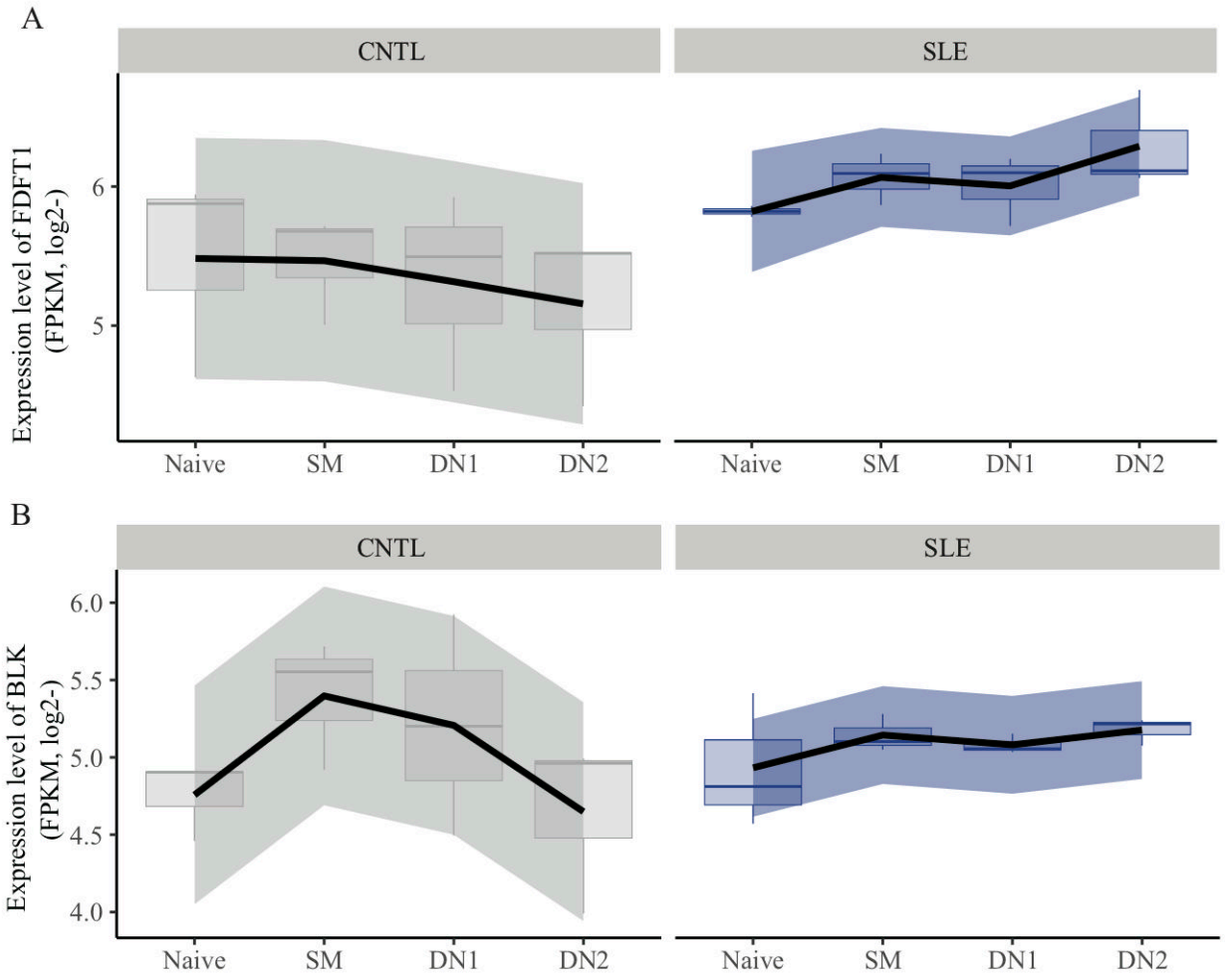

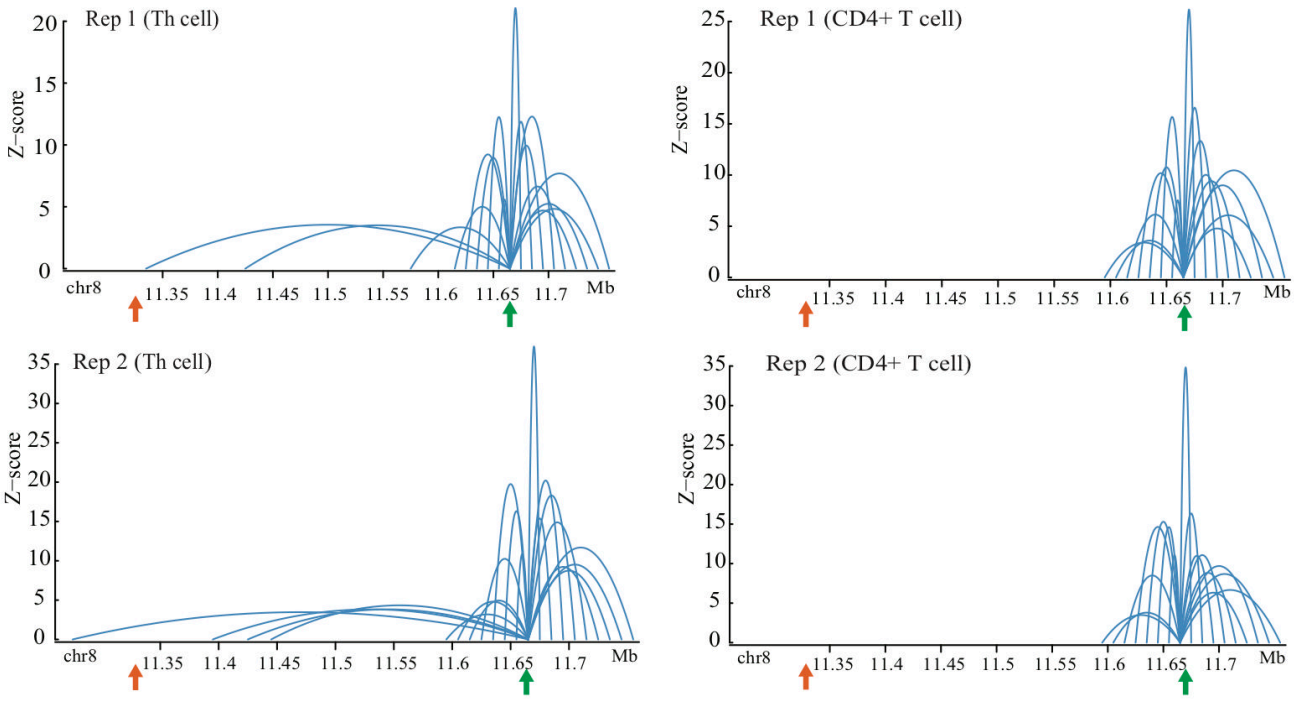

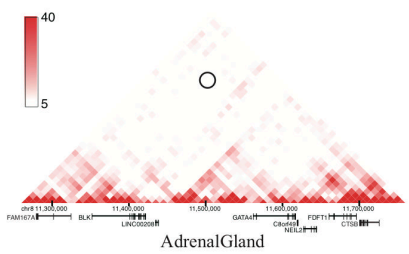

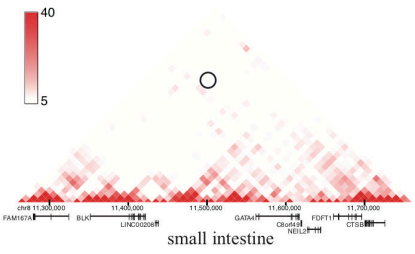

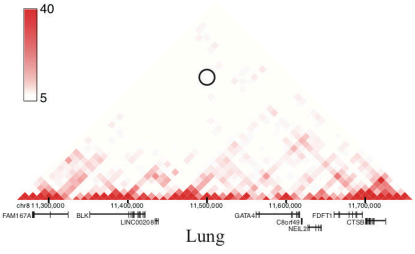

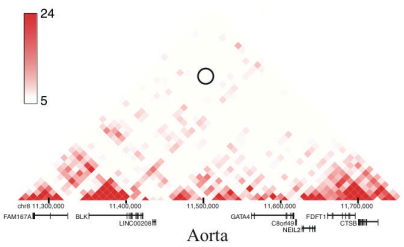

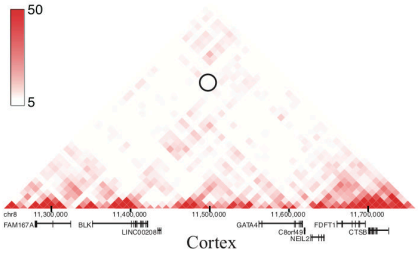

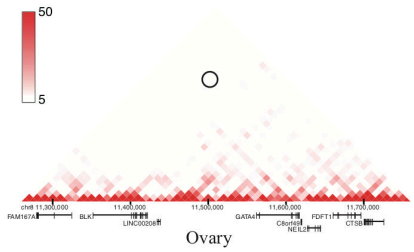

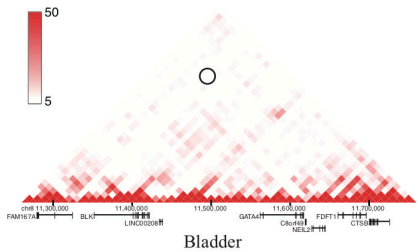

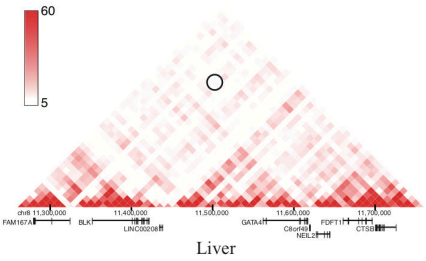

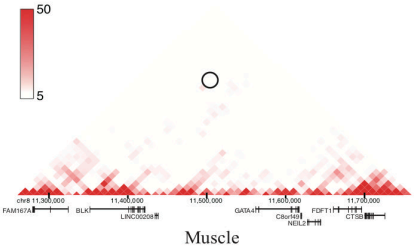

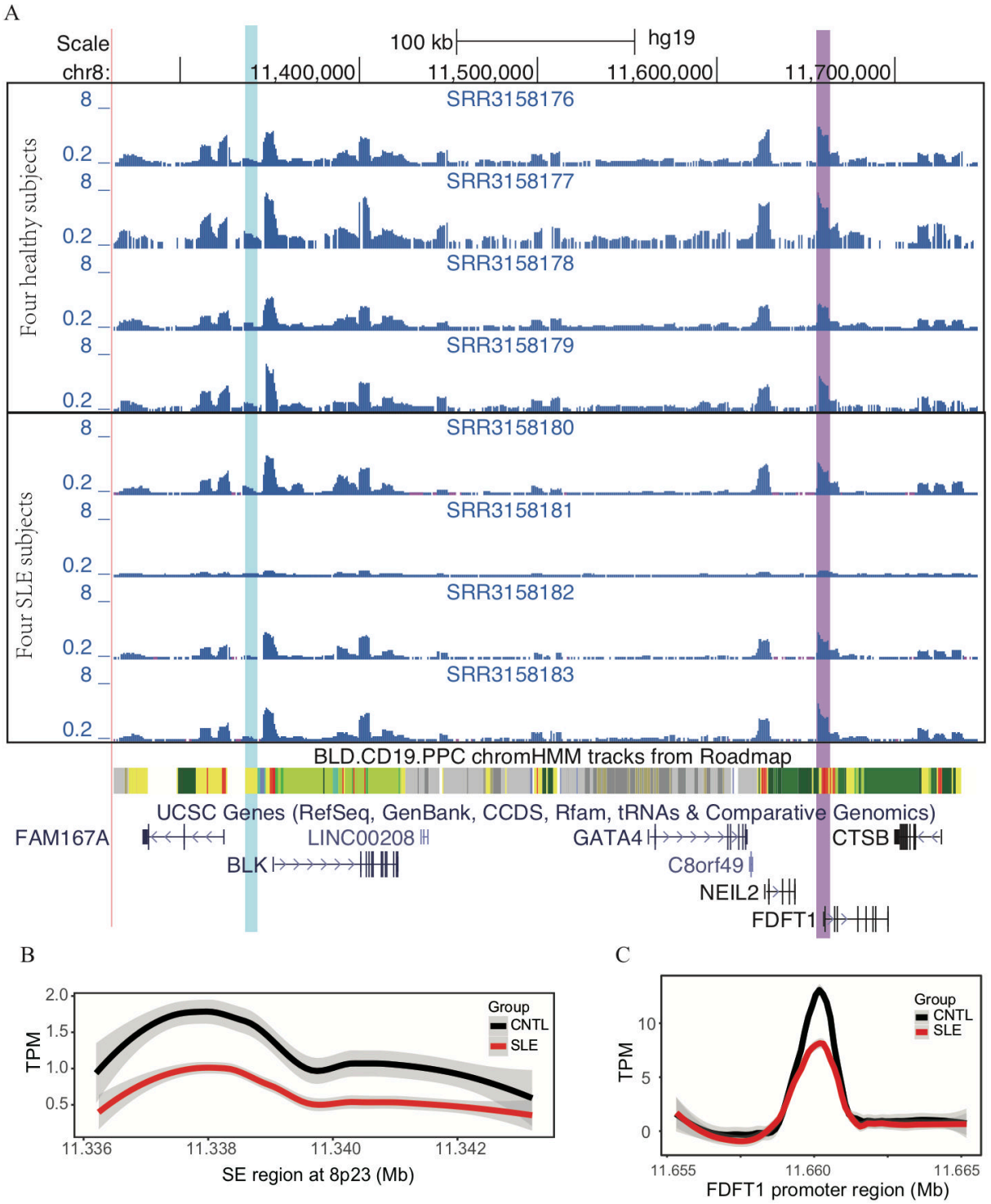

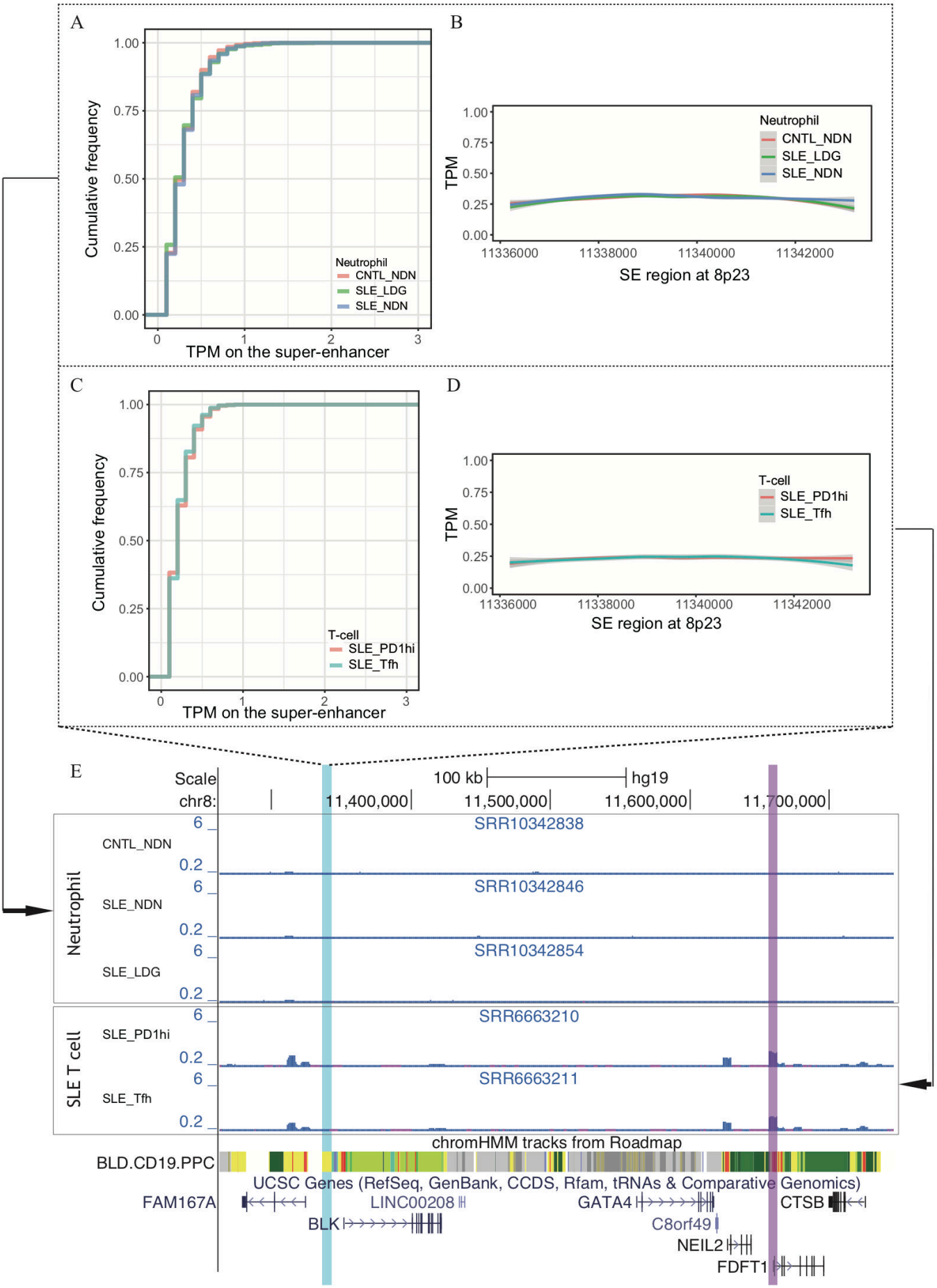

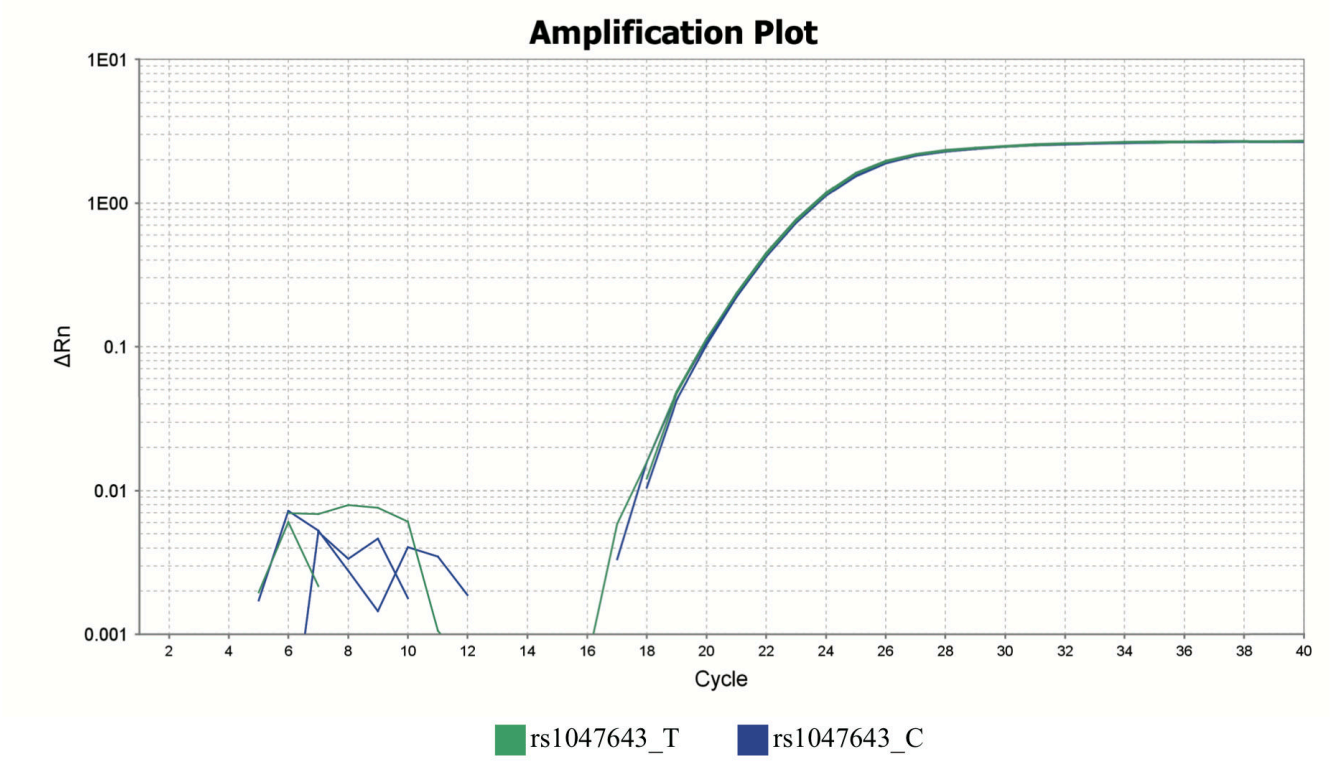

Stage	Data set (Accession ID)	Data description	Method	Samples, n (SLE vs Control)	Main Purpose
I					
	GSE118253	ATAC-Seq data in B cell subsets from a SLE case-control study	ATAC-seq	41 (14 vs 27)	Allelic imbalance analysis
	GSE71338	ATAC-Seq data in naive B cells from a SLE case-control study	ATAC-seq	8 (4 vs 4)	Allelic imbalance analysis
II					
	GSE139359	ATAC-Seq data in Neutrophil cells from a SLE case-control study	ATAC-seq	24 (16 vs 8)	Quantitative analysis of open chromatin regions
	GSE110017	ATAC-Seq data in two T cell subsets from a SLE study	ATAC-seq	6 (6 vs 0)	Quantitative analysis of open chromatin regions
	GSE118254	Transcriptomic data in B cell subsets from a SLE case-control study	RNA-seq	76 (42 vs 34)	Allelic expression analysis
	GSE92387	Transcriptomic data in B cell subsets from a SLE case-control study	RNA-seq	24 (12 vs 12)	Gene expression analysis
	GSE118255	DNA methylation data in B cell subsets from a SLE case-control study	RRBS-seq	85 (45 vs 40)	DNA methylation analysis
	GSE63525	Long-range chromatin interaction data on seven human cell types	Hi-C	7	Chromatin looping analysis
	GSE113405	Long-range chromatin interaction data in HepG2 cells	Hi-C	1	Chromatin looping analysis

GSE81503	DNA Looping Interactions in Capture Hi-C data in GM12878 cells	Capture Hi-C (CHi-C)	1	Chromatin looping analysis
E-MTAB-6621	DNA Looping Interactions in Capture Hi-C data in Tonsil-derived T-cells	Capture Hi-C (CHi-C)	6	Chromatin looping analysis
phs001025.v1	Hispanic Lupus GWAS Study	Microarray	2279 (1393 vs 886)	SNP association analysis

GSE ID	GSM ID	Group	Assay Type	Cell type
GSE118253	GSM3323580	CNTL	ATAC-seq	Activated Naive B cells (aN)
GSE118253	GSM3323581	CNTL	ATAC-seq	Double negative B cells (DN2)
GSE118253	GSM3323583	CNTL	ATAC-seq	Resting Naive B cells (rN)
GSE118253	GSM3323584	CNTL	ATAC-seq	Switched Memory B cells (SM)
GSE118253	GSM3323585	CNTL	ATAC-seq	Transitional 3 B cells (T3)
GSE118253	GSM3323586	CNTL	ATAC-seq	Double negative B cells (DN2)
GSE118253	GSM3323588	CNTL	ATAC-seq	Resting Naive B cells (rN)
GSE118253	GSM3323589	CNTL	ATAC-seq	Activated Naive B cells (aN)
GSE118253	GSM3323590	CNTL	ATAC-seq	Double negative B cells (DN2)
GSE118253	GSM3323592	CNTL	ATAC-seq	Resting Naive B cells (rN)
GSE118253	GSM3323593	CNTL	ATAC-seq	Switched Memory B cells (SM)
GSE118253	GSM3323594	CNTL	ATAC-seq	Transitional 3 B cells (T3)
GSE118253	GSM3323596	CNTL	ATAC-seq	Resting Naive B cells (rN)
GSE118253	GSM3323597	CNTL	ATAC-seq	Transitional 3 B cells (T3)
GSE118253	GSM3323598	CNTL	ATAC-seq	Double negative B cells (DN2)
GSE118253	GSM3323600	CNTL	ATAC-seq	Switched Memory B cells (SM)
GSE118253	GSM3323601	CNTL	ATAC-seq	Transitional 3 B cells (T3)
GSE118253	GSM3323602	CNTL	ATAC-seq	Activated Naive B cells (aN)
GSE118253	GSM3323604	CNTL	ATAC-seq	Switched Memory B cells (SM)
GSE118253	GSM3323605	CNTL	ATAC-seq	Transitional 3 B cells (T3)
GSE118253	GSM3323606	CNTL	ATAC-seq	Double negative B cells (DN2)
GSE118253	GSM3323608	CNTL	ATAC-seq	Switched Memory B cells (SM)
GSE118253	GSM3323609	CNTL	ATAC-seq	Transitional 3 B cells (T3)
GSE118253	GSM3323610	CNTL	ATAC-seq	Activated Naive B cells (aN)
GSE118253	GSM3323611	CNTL	ATAC-seq	Double negative B cells (DN2)
GSE118253	GSM3323613	CNTL	ATAC-seq	Switched Memory B cells (SM)
GSE118253	GSM3323614	CNTL	ATAC-seq	Transitional 3 B cells (T3)
GSE118253	GSM3323615	SLE	ATAC-seq	Activated Naive B cells (aN)
GSE118253	GSM3323616	SLE	ATAC-seq	Double negative B cells (DN2)
GSE118253	GSM3323617	SLE	ATAC-seq	Switched Memory B cells (SM)

GSE118253	GSM3323618	SLE	ATAC-seq	Transitional 3 B cells (T3)
GSE118253	GSM3323619	SLE	ATAC-seq	Activated Naive B cells (aN)
GSE118253	GSM3323620	SLE	ATAC-seq	Double negative B cells (DN2)
GSE118253	GSM3323621	SLE	ATAC-seq	Switched Memory B cells (SM)
GSE118253	GSM3323622	SLE	ATAC-seq	Transitional 3 B cells (T3)
GSE118253	GSM3323623	SLE	ATAC-seq	Double negative B cells (DN2)
GSE118253	GSM3323624	SLE	ATAC-seq	Switched Memory B cells (SM)
GSE118253	GSM3323625	SLE	ATAC-seq	Activated Naive B cells (aN)
GSE118253	GSM3323626	SLE	ATAC-seq	Double negative B cells (DN2)
GSE118253	GSM3323628	SLE	ATAC-seq	Switched Memory B cells (SM)
GSE118253	GSM3323629	SLE	ATAC-seq	Transitional 3 B cells (T3)
GSE71338	GSM2058522	CNTL	ATAC-Seq	Naive B cell
GSE71338	GSM2058523	CNTL	ATAC-Seq	Naive B cell
GSE71338	GSM2058524	CNTL	ATAC-Seq	Naive B cell
GSE71338	GSM2058525	CNTL	ATAC-Seq	Naive B cell
GSE71338	GSM2058526	SLE	ATAC-Seq	Naive B cell
GSE71338	GSM2058527	SLE	ATAC-Seq	Naive B cell
GSE71338	GSM2058528	SLE	ATAC-Seq	Naive B cell
GSE71338	GSM2058529	SLE	ATAC-Seq	Naive B cell
GSE118254	GSM3323630	Control	RNA-Seq	Activated Naive B cells (aN)
GSE118254	GSM3323631	Control	RNA-Seq	Double negative B cells (DN2)
GSE118254	GSM3323632	Control	RNA-Seq	Switched Memory B cells (SM)
GSE118254	GSM3323633	Control	RNA-Seq	Transitional 3 B cells (T3)
GSE118254	GSM3323634	Control	RNA-Seq	Resting Naive B cells (rN)
GSE118254	GSM3323635	Control	RNA-Seq	Switched Memory B cells (SM)
GSE118254	GSM3323636	Control	RNA-Seq	Transitional 3 B cells (T3)
GSE118254	GSM3323637	Control	RNA-Seq	Double negative B cells (DN2)
GSE118254	GSM3323638	Control	RNA-Seq	Resting Naive B cells (rN)
GSE118254	GSM3323639	Control	RNA-Seq	Switched Memory B cells (SM)
GSE118254	GSM3323640	Control	RNA-Seq	Transitional 3 B cells (T3)
GSE118254	GSM3323641	Control	RNA-Seq	Activated Naive B cells (aN)

GSE118254	GSM3323642	Control	RNA-Seq	Double negative B cells (DN2)
GSE118254	GSM3323644	Control	RNA-Seq	Resting Naive B cells (rN)
GSE118254	GSM3323645	Control	RNA-Seq	Switched Memory B cells (SM)
GSE118254	GSM3323646	Control	RNA-Seq	Transitional 3 B cells (T3)
GSE118254	GSM3323647	Control	RNA-Seq	Activated Naive B cells (aN)
GSE118254	GSM3323648	Control	RNA-Seq	Switched Memory B cells (SM)
GSE118254	GSM3323649	Control	RNA-Seq	Transitional 3 B cells (T3)
GSE118254	GSM3323650	Control	RNA-Seq	Activated Naive B cells (aN)
GSE118254	GSM3323651	Control	RNA-Seq	Double negative B cells (DN2)
GSE118254	GSM3323652	Control	RNA-Seq	Resting Naive B cells (rN)
GSE118254	GSM3323653	Control	RNA-Seq	Switched Memory B cells (SM)
GSE118254	GSM3323654	Control	RNA-Seq	Transitional 3 B cells (T3)
GSE118254	GSM3323655	Control	RNA-Seq	Activated Naive B cells (aN)
GSE118254	GSM3323656	Control	RNA-Seq	Double negative B cells (DN2)
GSE118254	GSM3323658	Control	RNA-Seq	Resting Naive B cells (rN)
GSE118254	GSM3323660	Control	RNA-Seq	Transitional 3 B cells (T3)
GSE118254	GSM3323659	Control	RNA-Seq	Switched Memory B cells (SM)
GSE118254	GSM3323661	Control	RNA-Seq	Activated Naive B cells (aN)
GSE118254	GSM3323662	Control	RNA-Seq	Double negative B cells (DN2)
GSE118254	GSM3323664	Control	RNA-Seq	Resting Naive B cells (rN)
GSE118254	GSM3323665	Control	RNA-Seq	Switched Memory B cells (SM)
GSE118254	GSM3323666	Control	RNA-Seq	Transitional 3 B cells (T3)
GSE118254	GSM3323667	SLE	RNA-Seq	Activated Naive B cells (aN)
GSE118254	GSM3323668	SLE	RNA-Seq	Double negative B cells (DN2)
GSE118254	GSM3323670	SLE	RNA-Seq	Resting Naive B cells (rN)
GSE118254	GSM3323671	SLE	RNA-Seq	Switched Memory B cells (SM)
GSE118254	GSM3323672	SLE	RNA-Seq	Transitional 3 B cells (T3)
GSE118254	GSM3323673	SLE	RNA-Seq	Activated Naive B cells (aN)
GSE118254	GSM3323674	SLE	RNA-Seq	Double negative B cells (DN2)
GSE118254	GSM3323675	SLE	RNA-Seq	Resting Naive B cells (rN)
GSE118254	GSM3323676	SLE	RNA-Seq	Switched Memory B cells (SM)

GSE118254	GSM3323677	SLE	RNA-Seq	Transitional 3 B cells (T3)
GSE118254	GSM3323678	SLE	RNA-Seq	Activated Naive B cells (aN)
GSE118254	GSM3323679	SLE	RNA-Seq	Double negative B cells (DN2)
GSE118254	GSM3323681	SLE	RNA-Seq	Resting Naive B cells (rN)
GSE118254	GSM3323682	SLE	RNA-Seq	Switched Memory B cells (SM)
GSE118254	GSM3323683	SLE	RNA-Seq	Transitional 3 B cells (T3)
GSE118254	GSM3323684	SLE	RNA-Seq	Activated Naive B cells (aN)
GSE118254	GSM3323685	SLE	RNA-Seq	Double negative B cells (DN2)
GSE118254	GSM3323688	SLE	RNA-Seq	Switched Memory B cells (SM)
GSE118254	GSM3323687	SLE	RNA-Seq	Resting Naive B cells (rN)
GSE118254	GSM3323689	SLE	RNA-Seq	Transitional 3 B cells (T3)
GSE118254	GSM3323690	SLE	RNA-Seq	Activated Naive B cells (aN)
GSE118254	GSM3323691	SLE	RNA-Seq	Double negative B cells (DN2)
GSE118254	GSM3323692	SLE	RNA-Seq	Resting Naive B cells (rN)
GSE118254	GSM3323694	SLE	RNA-Seq	Transitional 3 B cells (T3)
GSE118254	GSM3323693	SLE	RNA-Seq	Switched Memory B cells (SM)
GSE118254	GSM3323695	SLE	RNA-Seq	Switched Memory B cells (SM)
GSE118254	GSM3323696	SLE	RNA-Seq	Transitional 3 B cells (T3)
GSE118254	GSM3323697	SLE	RNA-Seq	Activated Naive B cells (aN)
GSE118254	GSM3323699	SLE	RNA-Seq	Resting Naive B cells (rN)
GSE118254	GSM3323698	SLE	RNA-Seq	Double negative B cells (DN2)
GSE118254	GSM3323700	SLE	RNA-Seq	Switched Memory B cells (SM)
GSE118254	GSM3323701	SLE	RNA-Seq	Transitional 3 B cells (T3)
GSE118254	GSM3323702	SLE	RNA-Seq	Double negative B cells (DN2)
GSE118254	GSM3323704	SLE	RNA-Seq	Switched Memory B cells (SM)
GSE118254	GSM3323703	SLE	RNA-Seq	Resting Naive B cells (rN)
GSE118254	GSM3323705	SLE	RNA-Seq	Transitional 3 B cells (T3)
GSE118254	GSM3323706	SLE	RNA-Seq	Resting Naive B cells (rN)
GSE118254	GSM3323707	SLE	RNA-Seq	Activated Naive B cells (aN)
GSE118254	GSM3323708	SLE	RNA-Seq	Double negative B cells (DN2)
GSE118254	GSM3323710	SLE	RNA-Seq	Resting Naive B cells (rN)

GSE118254	GSM3323711	SLE	RNA-Seq	Switched Memory B cells (SM)
GSE118254	GSM3323712	SLE	RNA-Seq	Transitional 3 B cells (T3)
GSE92387	GSM2428862	SLE	RNA-Seq	Naïve B cell
GSE92387	GSM2428863	SLE	RNA-Seq	Switched memory
GSE92387	GSM2428864	SLE	RNA-Seq	Double negative 1
GSE92387	GSM2428865	SLE	RNA-Seq	Double negative 2
GSE92387	GSM2428866	SLE	RNA-Seq	Naïve
GSE92387	GSM2428867	SLE	RNA-Seq	Switched memory
GSE92387	GSM2428868	SLE	RNA-Seq	Double negative 1
GSE92387	GSM2428869	SLE	RNA-Seq	Double negative 2
GSE92387	GSM2428870	SLE	RNA-Seq	Naïve
GSE92387	GSM2428871	SLE	RNA-Seq	Switched memory
GSE92387	GSM2428872	SLE	RNA-Seq	Double negative 1
GSE92387	GSM2428873	SLE	RNA-Seq	Double negative 2
GSE92387	GSM2428874	CNTL	RNA-Seq	Naïve
GSE92387	GSM2428875	CNTL	RNA-Seq	Switched memory
GSE92387	GSM2428876	CNTL	RNA-Seq	Double negative 1
GSE92387	GSM2428877	CNTL	RNA-Seq	Double negative 2
GSE92387	GSM2428878	CNTL	RNA-Seq	Naïve
GSE92387	GSM2428879	CNTL	RNA-Seq	Switched memory
GSE92387	GSM2428880	CNTL	RNA-Seq	Double negative 1
GSE92387	GSM2428881	CNTL	RNA-Seq	Double negative 2
GSE92387	GSM2428882	CNTL	RNA-Seq	Naïve
GSE92387	GSM2428883	CNTL	RNA-Seq	Switched memory
GSE92387	GSM2428884	CNTL	RNA-Seq	Double negative 1
GSE92387	GSM2428885	CNTL	RNA-Seq	Double negative 2
GSE139359	GSM4138735	CNTL	ATAC-seq	NDN
GSE139359	GSM4138736	CNTL	ATAC-seq	NDN
GSE139359	GSM4138737	CNTL	ATAC-seq	NDN
GSE139359	GSM4138738	CNTL	ATAC-seq	NDN
GSE139359	GSM4138739	CNTL	ATAC-seq	NDN

GSE139359	GSM4138740	CNTL	ATAC-seq	NDN
GSE139359	GSM4138741	CNTL	ATAC-seq	NDN
GSE139359	GSM4138742	CNTL	ATAC-seq	NDN
GSE139359	GSM4138743	SLE	ATAC-seq	NDN
GSE139359	GSM4138744	SLE	ATAC-seq	NDN
GSE139359	GSM4138745	SLE	ATAC-seq	NDN
GSE139359	GSM4138746	SLE	ATAC-seq	NDN
GSE139359	GSM4138747	SLE	ATAC-seq	NDN
GSE139359	GSM4138748	SLE	ATAC-seq	NDN
GSE139359	GSM4138749	SLE	ATAC-seq	NDN
GSE139359	GSM4138750	SLE	ATAC-seq	NDN
GSE139359	GSM4138751	SLE	ATAC-seq	LDG
GSE139359	GSM4138752	SLE	ATAC-seq	LDG
GSE139359	GSM4138753	SLE	ATAC-seq	LDG
GSE139359	GSM4138754	SLE	ATAC-seq	LDG
GSE139359	GSM4138755	SLE	ATAC-seq	LDG
GSE139359	GSM4138756	SLE	ATAC-seq	LDG
GSE139359	GSM4138757	SLE	ATAC-seq	LDG
GSE139359	GSM4138758	SLE	ATAC-seq	LDG
GSE110017	GSM2976426	SLE	ATAC-seq	CD4+ T (PD1hi)
GSE110017	GSM2976427	SLE	ATAC-seq	CD4+ T (Tfh)
GSE110017	GSM2976428	SLE	ATAC-seq	CD4+ T (PD1hi)
GSE110017	GSM2976429	SLE	ATAC-seq	CD4+ T (PD1hi)
GSE110017	GSM2976430	SLE	ATAC-seq	CD4+ T (Tfh)
GSE110017	GSM2976431	SLE	ATAC-seq	CD4+ T (PD1hi)
GSE118255	GSM3323713	CNTL	RRBS	Activated Naive B cells (aN)
GSE118255	GSM3323714	CNTL	RRBS	Double negative B cells (DN2)
GSE118255	GSM3323715	CNTL	RRBS	Resting Naive B cells (rN)
GSE118255	GSM3323716	CNTL	RRBS	Switched Memory B cells (SM)
GSE118255	GSM3323717	CNTL	RRBS	Transitional 3 B cells (T3)
GSE118255	GSM3323718	CNTL	RRBS	Activated Naive B cells (aN)

GSE118255	GSM3323719	CNTL	RRBS	Double negative B cells (DN2)
GSE118255	GSM3323720	CNTL	RRBS	Resting Naive B cells (rN)
GSE118255	GSM3323721	CNTL	RRBS	Switched Memory B cells (SM)
GSE118255	GSM3323722	CNTL	RRBS	Transitional 3 B cells (T3)
GSE118255	GSM3323723	CNTL	RRBS	Activated Naive B cells (aN)
GSE118255	GSM3323724	CNTL	RRBS	Double negative B cells (DN2)
GSE118255	GSM3323725	CNTL	RRBS	Resting Naive B cells (rN)
GSE118255	GSM3323726	CNTL	RRBS	Switched Memory B cells (SM)
GSE118255	GSM3323727	CNTL	RRBS	Transitional 3 B cells (T3)
GSE118255	GSM3323728	CNTL	RRBS	Activated Naive B cells (aN)
GSE118255	GSM3323729	CNTL	RRBS	Double negative B cells (DN2)
GSE118255	GSM3323730	CNTL	RRBS	Resting Naive B cells (rN)
GSE118255	GSM3323731	CNTL	RRBS	Switched Memory B cells (SM)
GSE118255	GSM3323732	CNTL	RRBS	Transitional 3 B cells (T3)
GSE118255	GSM3323733	CNTL	RRBS	Activated Naive B cells (aN)
GSE118255	GSM3323734	CNTL	RRBS	Double negative B cells (DN2)
GSE118255	GSM3323736	CNTL	RRBS	Resting Naive B cells (rN)
GSE118255	GSM3323737	CNTL	RRBS	Switched Memory B cells (SM)
GSE118255	GSM3323738	CNTL	RRBS	Transitional 3 B cells (T3)
GSE118255	GSM3323739	CNTL	RRBS	Activated Naive B cells (aN)
GSE118255	GSM3323740	CNTL	RRBS	Double negative B cells (DN2)
GSE118255	GSM3323741	CNTL	RRBS	Resting Naive B cells (rN)
GSE118255	GSM3323742	CNTL	RRBS	Switched Memory B cells (SM)
GSE118255	GSM3323743	CNTL	RRBS	Transitional 3 B cells (T3)
GSE118255	GSM3323744	CNTL	RRBS	Activated Naive B cells (aN)
GSE118255	GSM3323745	CNTL	RRBS	Double negative B cells (DN2)
GSE118255	GSM3323747	CNTL	RRBS	Resting Naive B cells (rN)
GSE118255	GSM3323748	CNTL	RRBS	Switched Memory B cells (SM)
GSE118255	GSM3323749	CNTL	RRBS	Transitional 3 B cells (T3)
GSE118255	GSM3323750	CNTL	RRBS	Activated Naive B cells (aN)
GSE118255	GSM3323751	CNTL	RRBS	Double negative B cells (DN2)

GSE118255	GSM3323753	CNTL	RRBS	Resting Naive B cells (rN)
GSE118255	GSM3323754	CNTL	RRBS	Switched Memory B cells (SM)
GSE118255	GSM3323755	CNTL	RRBS	Transitional 3 B cells (T3)
GSE118255	GSM3323756	SLE	RRBS	Activated Naive B cells (aN)
GSE118255	GSM3323757	SLE	RRBS	Double negative B cells (DN2)
GSE118255	GSM3323758	SLE	RRBS	Resting Naive B cells (rN)
GSE118255	GSM3323759	SLE	RRBS	Switched Memory B cells (SM)
GSE118255	GSM3323760	SLE	RRBS	Transitional 3 B cells (T3)
GSE118255	GSM3323761	SLE	RRBS	Activated Naive B cells (aN)
GSE118255	GSM3323762	SLE	RRBS	Double negative B cells (DN2)
GSE118255	GSM3323763	SLE	RRBS	Resting Naive B cells (rN)
GSE118255	GSM3323764	SLE	RRBS	Switched Memory B cells (SM)
GSE118255	GSM3323765	SLE	RRBS	Transitional 3 B cells (T3)
GSE118255	GSM3323766	SLE	RRBS	Activated Naive B cells (aN)
GSE118255	GSM3323767	SLE	RRBS	Double negative B cells (DN2)
GSE118255	GSM3323768	SLE	RRBS	Resting Naive B cells (rN)
GSE118255	GSM3323769	SLE	RRBS	Switched Memory B cells (SM)
GSE118255	GSM3323770	SLE	RRBS	Transitional 3 B cells (T3)
GSE118255	GSM3323771	SLE	RRBS	Activated Naive B cells (aN)
GSE118255	GSM3323772	SLE	RRBS	Double negative B cells (DN2)
GSE118255	GSM3323773	SLE	RRBS	Resting Naive B cells (rN)
GSE118255	GSM3323774	SLE	RRBS	Switched Memory B cells (SM)
GSE118255	GSM3323775	SLE	RRBS	Transitional 3 B cells (T3)
GSE118255	GSM3323776	SLE	RRBS	Activated Naive B cells (aN)
GSE118255	GSM3323777	SLE	RRBS	Double negative B cells (DN2)
GSE118255	GSM3323779	SLE	RRBS	Resting Naive B cells (rN)
GSE118255	GSM3323780	SLE	RRBS	Switched Memory B cells (SM)
GSE118255	GSM3323781	SLE	RRBS	Transitional 3 B cells (T3)
GSE118255	GSM3323782	SLE	RRBS	Activated Naive B cells (aN)
GSE118255	GSM3323783	SLE	RRBS	Double negative B cells (DN2)
GSE118255	GSM3323784	SLE	RRBS	Resting Naive B cells (rN)

GSE118255	GSM3323785	SLE	RRBS	Switched Memory B cells (SM)
GSE118255	GSM3323786	SLE	RRBS	Transitional 3 B cells (T3)
GSE118255	GSM3323787	SLE	RRBS	Activated Naive B cells (aN)
GSE118255	GSM3323788	SLE	RRBS	Double negative B cells (DN2)
GSE118255	GSM3323790	SLE	RRBS	Resting Naive B cells (rN)
GSE118255	GSM3323791	SLE	RRBS	Switched Memory B cells (SM)
GSE118255	GSM3323792	SLE	RRBS	Transitional 3 B cells (T3)
GSE118255	GSM3323793	SLE	RRBS	Activated Naive B cells (aN)
GSE118255	GSM3323794	SLE	RRBS	Double negative B cells (DN2)
GSE118255	GSM3323796	SLE	RRBS	Resting Naive B cells (rN)
GSE118255	GSM3323797	SLE	RRBS	Switched Memory B cells (SM)
GSE118255	GSM3323798	SLE	RRBS	Transitional 3 B cells (T3)
GSE118255	GSM3323799	SLE	RRBS	Activated Naive B cells (aN)
GSE118255	GSM3323800	SLE	RRBS	Double negative B cells (DN2)
GSE118255	GSM3323802	SLE	RRBS	Resting Naive B cells (rN)
GSE118255	GSM3323803	SLE	RRBS	Switched Memory B cells (SM)
GSE118255	GSM3323804	SLE	RRBS	Transitional 3 B cells (T3)

Primer name	Strand	Sequence	Purpose
GAPDH	Forward	TCACCAGGGCTGCTTTTAAC	RT-qPCR
	Reverse	TGACGGTGCCATGGAATTTG	
FDFT1	Forward	GACCAGCAAGGAGGAAGAGAG	RT-qPCR
	Reverse	CCAAGTCAATATTCTCCGGCT	
BLK	Forward	CTTGCTCCAATCAACAAGGC	RT-qPCR
	Reverse	TAGTGCTTGATCAGCTCCCC	
rs1047643 allelic	Forward 1	TGGAGTTCGTGAAATGCCTT	Allelic qPCR
	Forward 2	TGGAGTTCGTGAAATGCCTC	
	Reverse	CAAGCAGGGAGGCTCGG	
SE5term_8p23	Forward	GGATGGATCTGCTGCCTTGT	ChIP qPCR
	Reverse	GCTGCTGGTGGGTGTTTTC	
SE3term_8p23	Forward	TGGGGTGTTGAAGGCTGAAA	ChIP qPCR
	Reverse	CGGTGGGTAAGCAGTGTACT	